


Review

# Characterization of Wax Precipitation and Deposition Behavior of Condensate Oil in Wellbore: A Comprehensive Review of Modeling, Experiment, and Molecular Dynamics Simulation

Yong Wang<sup>1</sup>, Xiaoyu Liu<sup>1</sup>, Zuonan Huang<sup>2</sup>, Zhihua Wang<sup>1</sup>  and Yang Liu<sup>1,\*</sup>

<sup>1</sup> Key Laboratory for Enhanced Oil & Gas Recovery of the Ministry of Education, Northeast Petroleum University, Daqing 163318, China; wydqpi@126.com (Y.W.); lxljy160930@163.com (X.L.); zhihua\_wang@126.com (Z.W.)

<sup>2</sup> Oil Recovery Plant No. 4, PetroChina Daqing Oilfield Company Limited, Daqing 163511, China; huangzn1995@163.com

\* Correspondence: lynepu@163.com; Tel.: +86-459-650-3330

**Abstract:** Condensate oil is increasingly valued as the high-quality conventional hydrocarbon resources generally decline. The efficient development of condensate oil, however, has always been a world problem; massive condensate oil will be retained in reservoirs in case of improper exploitation process, resulting in a significant resource waste and economic loss. One of the problems closely related to enhancing condensate oil recovery is wax precipitation and deposition in wellbore. Therefore, it is vital to investigate the characterization methods for the wax precipitation and deposition behavior in wellbores. The current status of research on modelling characterization methods, experimental characterization methods and molecular dynamics representation of wax precipitation and deposition behavior is reviewed in this paper; the applicability and limitation of modeling and experiment studies for characterizing wax precipitation and deposition of condensate oil in the wellbore are critically summarized and discussed. Moreover, the molecular dynamics simulation technique characterizes wax precipitation and deposition behavior from the micro scale, which makes up for the deficiencies of macroscopic experiment, enriches the investigation of wax precipitation and deposition, and provides important guidance and reference value for the development of unconventional hydrocarbon exploitation processes.

**Keywords:** condensate oil; wellbore blockage; multiphase flow; wax precipitation and deposition; characterization method; molecular dynamics simulation



**Citation:** Wang, Y.; Liu, X.; Huang, Z.; Wang, Z.; Liu, Y. Characterization of Wax Precipitation and Deposition Behavior of Condensate Oil in Wellbore: A Comprehensive Review of Modeling, Experiment, and Molecular Dynamics Simulation. *Energies* **2022**, *15*, 4018. <https://doi.org/10.3390/en15114018>

Academic Editors: Galih Bangga, Mofazzal Hossain and Noam Lior

Received: 31 March 2022

Accepted: 27 May 2022

Published: 30 May 2022

**Publisher's Note:** MDPI stays neutral with regard to jurisdictional claims in published maps and institutional affiliations.



**Copyright:** © 2022 by the authors. Licensee MDPI, Basel, Switzerland. This article is an open access article distributed under the terms and conditions of the Creative Commons Attribution (CC BY) license (<https://creativecommons.org/licenses/by/4.0/>).

## 1. Introduction

With the further deepening of global hydrocarbon exploration, high-quality shallow hydrocarbon resources are increasingly becoming scarce, and the unconventional and deep hydrocarbon resources are gradually becoming vital in the energy structure [1,2]. While continuing to strengthen the exploration and development of conventional crude oil, emphasis should also be placed on accelerating the development of superior resources such as light oil and condensate oil [3,4]. Condensate oil is a colorless and transparent liquid phase component condensed from natural gas in condensate fields or associated gas in oil fields. The main composition is a mixture of C<sub>5</sub>~C<sub>8</sub> hydrocarbons and contains modicum hydrocarbons larger than C<sub>8</sub> as well as impurities such as sulfur dioxide, thiophenes, mercaptans, sulfur ethers, and polysulfides, and its heavy hydrocarbon and non-hydrocarbon fractions are lower than that of conventional crude oil [5–7]. Large condensate fields have been discovered in over 60 countries and regions worldwide, mainly in the United States, Russia, and the Middle East. Condensate resources are also quite abundant in China, and the existence of condensate reservoirs has been successively proven in major oil fields [8,9]. However, different from conventional reservoirs, the condensate reservoirs are deeply

buried and hydrocarbon accumulation is subjected to harsh temperature and pressure environments, resulting in great difficulty in exploitation.

Waxes are present in condensate oil developed in most countries around the world and exist in various phase states (gas, liquid and solid) depending on temperature and pressure [9–12]. Macrocrystalline and microcrystalline waxes, which are key components of waxy condensate oil, have very different functional properties, including viscosity and melting point [13,14]. Oliveira et al. [15] found through their investigations that although the structure of microcrystalline wax is smaller and thinner than macrocrystalline wax, it was much more difficult to remove from the pipe wall or wellbore wall than macrocrystalline wax. The waxes dissolved in the condensate oil in molecular form undergo a series of processes such as diffusion, aggregation, and phase transition due to changes in the external environment [16]. The properties of the wax crystals are very complex, and the precipitated wax crystals are gradually deposited on the wellbore wall, which reduces the effective flow area of the wellbore [17,18]. At the same time, it will also cause deterioration of the rheological properties of condensate oil, even lead to wellbore blockage, and finally engender serious production and economic losses [19,20]. The schematic diagram of wax precipitation and deposition in the wellbore is shown in Figure 1. Several observations from the industrial field have shown that the formation frequency of wax has been high in condensate oil over the past few decades. The condensate oil production of Miller oilfield in the North Sea dropped sharply from 30,000 barrels per day to zero within 24 h; this could be attributed to the fact that the serious wax blockage occurred in the wellbore during the condensate oil development [21]. Due to the high wax content in the South Pars condensate field in Iran, the wax precipitation and deposition in the process of condensate recovery led to a narrower wellbore diameter, a high flow resistance and a sharp drop in production. In the gathering and transportation process of produced mixed multiphase liquid, the precipitation of a large number of wax crystals was attributed to the low environment temperature, which gelled with each other to form a mesh structure and had an obstructive effect on the transport of the oil and gas multiphase mixtures. As the transportation distance and environment varied, the network structure increasingly expanded, and the wax molecules formed a dense wax layer inside the pipe wall due to their own gravity, which led to the obstruction of condensate hydrocarbons transportation and sale channels [22]. In the production process of condensate oil wells in the Boz block of Tarim Oilfield in China, only ten days after well opening, the wells were shut down due to wax blockage, which seriously caused the normal production of hydrocarbon wells [12]. Arguably the most serious incident of wax deposition causing wellbore blockage might have occurred at the Staffa Field, Block 3/8b, UK North Sea. After several failed attempts to deal with the wax deposit problem in this field, the field and its platform were eventually abandoned and the loss was estimated to be as high as \$1 billion [23]. Therefore, the wax precipitation and deposition of condensate oil in the wellbore has become a relevant issue that needs to be urgently addressed. Multi-level revealing and characterizing the wax precipitation and deposition behavior is the key to ensuring the safe and efficient operation of surface systems, developing enhanced condensate oil recovery technology, and designing wax prevention and removal technology development [24].

This paper reviews the current status of modeling and experiment research to characterize the wax precipitation and deposition behavior of condensate oil in the wellbore. The applicability of molecular dynamics (MD) simulation to microstructural characterization makes such simulations well suited for revealing phase transition and solid phase deposition. The research progress of MD in characterizing wax precipitation and deposition behavior is discussed to deepen our microscopic-scale understanding of phenomena determining the wax molecule phase transition, wax precipitation, and wax deposition process. Future applications and development directions of MD simulation methods in characterizing wax precipitation and deposition behavior of condensate oil in the wellbore are put forward to provide a reference for enriching the theoretical understanding of the

wax formation process and promoting the development of unconventional hydrocarbon production and transportation technologies.

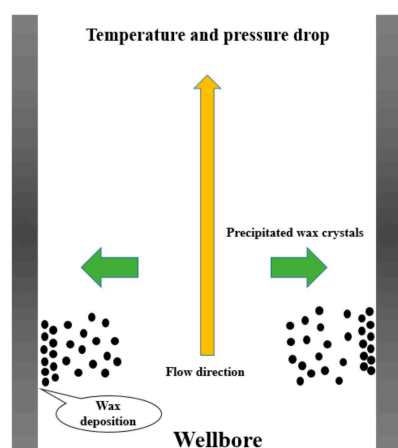


Figure 1. The schematic diagram of wellbore wax precipitation and deposition [25].

## 2. Modeling Characterization of Wax Precipitation and Deposition Behavior

It is necessary to develop models to analyze and characterize wax precipitation and deposition behavior and to calculate relevant parameters such as wax precipitation temperature and amount, wax deposition thickness and rate, which is of great significance for mastering the wax deposition law and formulating a reasonable plugging removal scheme [26,27].

### 2.1. Modeling Characterization of Wax Precipitation Behavior

The modeling of wax precipitation is based on thermodynamic and kinetic equilibrium to describe the liquid-solid phase transition process of wax molecules [28–30]. Different from conventional crude oil, the condensate oil system has the highest wax precipitation temperature near the dew point pressure, this can be attributed to the fact that there are only heavy hydrocarbon components at the dew point, which decreases the wax solubility. When the pressure is higher than the dew point pressure, the content of heavy hydrocarbon components is low. With the increase in pressure, the wax components may dissolve in the gas phase, which decreases the wax precipitation temperature. When the pressure is lower than the dew point pressure, liquid hydrocarbon will appear. As the wax component condenses in the liquid phase, its solubility increases, and the wax precipitation temperature decreases [11,12,31,32]. The phase envelope of the typical condensate oil system is shown in Figure 2.

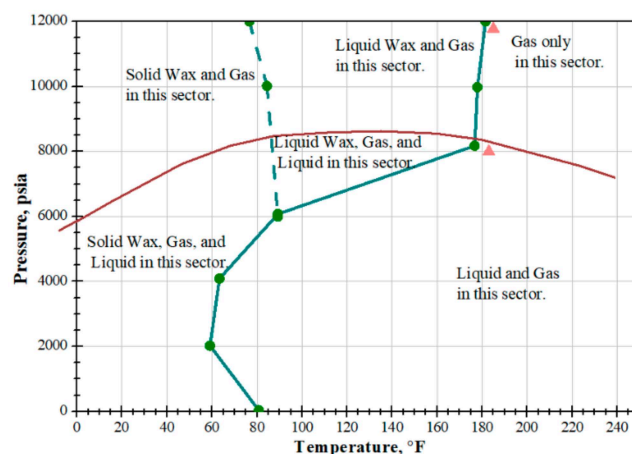


Figure 2. Phase envelope of a typical condensate oil system [21].

Generally, the theoretical basis for modeling is a solid solution and multiple solid theories [33–35]. Several representative models have been proposed to describe this behavior. Won et al. [36] first developed a model for condensate oil wax precipitation based on solid solution theory in 1986. The SRK equation and the modified regular solution theory were used to describe the non-ideality of the liquid phase, respectively. However, this lack of consistency in thermodynamics limits the prediction ability of this model. Subsequently, Thomas et al. [37] introduced the Poynting factor based on the Won model and considered the effect of pressure on the liquid-solid phase equilibrium. The wax precipitation model established by Lira-Galeana et al. [38] assumed that waxes contained multiple phases, each phase was described by pure component. Additionally, the amount of wax crystals precipitated from a condensate consisting of a mixture of six alkanes with a molar fraction of 400 was measured experimentally as a function of temperature. It was found that the predicted trend of solid content with temperature was in good agreement with the experimental results. However, Pedersen et al. later demonstrated that the model applicable conditions were limited. When the physical parameters of oil samples changed, the calculation results of the model fluctuated greatly. Therefore, Pedersen et al. [39] established a gas-liquid-solid three-phase wax precipitation model with thermodynamic consistency by modifying Won and Lira-Galeana models. The model assumed that wax was an ideal mixture, and only part of the pseudo-components can be regarded as wax. Precipitable and non-precipitable parts of pseudo-components above  $C_7$  can be derived from the following equation.

$$\begin{cases} z_i^S = z_i^{\text{tot}} \left[ 1 - (0.8824 + 5.353 \times 10^{-4} M_i) \left( \frac{\rho_i - \rho_i^P}{\rho_i^P} \right)^{0.1144} \right] \\ \rho_i^P = 0.3915 + 0.0675 \ln M_i \end{cases} \quad (1)$$

where  $z_i^{\text{tot}}$  is the total mole fraction of pseudo-component  $i$ ;  $z_i^S$  is the mole fraction of the potentially wax forming part of pseudo-component  $i$ ;  $\rho_i$  is the density at standard condition of total pseudo-component  $i$ ,  $\text{g}/\text{cm}^3$ ;  $\rho_i^P$  is the density at standard conditions of a normal wax with the same molecular weight as pseudo-component  $i$ ,  $\text{g}/\text{cm}^3$ ;  $M_i$  is the molecular weight of pseudo-component  $i$ ,  $\text{g}/\text{mol}$ . It was shown that the Pedersen model overcame the problem that the Won model severely overestimated the wax precipitation temperature and amount, and its prediction accuracy was higher.

Pan et al. [40] established a wax precipitation model of condensate oil system based on multiple solid theory and used PR state equation to describe the non-ideality of the liquid phase. Since the Lira-Galeana and Pedersen model is not applicable to calculate the wax precipitation characteristics directly through the average physical properties of pseudo-components. For this reason, the pseudo-components were reclassified and a set of physical property calculation formulas for alkanes, cycloalkanes, and aromatic hydrocarbons were given, respectively. In addition, the Pedersen and Pan models have some limitations in considering the effects of solid-phase composition and pressure on solid-phase non-ideality. Although the Won and Thomas models used the regular solution theory to calculate the solid activity coefficient, they ignored the contribution of excess entropy to excess Gibbs free energy.

Furthermore, Nichita [41,42], Daridon [43], Sansot [44], Coutinho [45], and Zuo et al. [46] have successively developed the wax precipitation model of condensate oil system with perfect theory and strong predictability. The effect of pressure on wax precipitation in condensate oil was considered in the Nichita model. The high-temperature and high-pressure environment was considered in modeling by Daridon et al., and the excess Gibbs free energy was calculated. The assumption that the precipitated solid phase consisted of only n-alkanes was considered in the Sansot model. In addition, the effect of pressure on solid-phase fugacity was reflected by the Poynting factor. The local component prediction model developed by Coutinho et al. could well predict the wax precipitation behavior of various oils. In two variant forms of the model, the wax phase was regarded as a single

solid solution of n-alkanes and multiple coexisting solid solutions. The effect of solid-phase composition on solid-phase fugacity was described separately in the model by Zuo et al.

## 2.2. Modeling Characterization of Wax Deposition Behavior

Wax deposition in the wellbore is a very complex process, which refers to the formation and eventual growth of a solid layer attached to the wellbore surface. It can be seen from Figure 2 that the condensate oil system has complex phase evolution characteristics in the wellbore, and wax deposition may occur in each phase. So far, scholars have conducted many studies on wax deposition in single-phase flow. Based on the support of laboratory test data, a series of typical models to characterize wax deposition behavior were proposed by Burger [47], Hamouda [48], Hsu [49], Ramírez-Jaramillo [50], and Singh et al. [51–53]. The summary of the wax deposition models is shown in Table 1.

**Table 1.** Summary of single-phase wax deposition models.

Researcher	Mechanism	Mathematical Model	Establishment and Characteristics of the Model
Burger [47]	MD, BD, SD	$W_t = \rho_r AD_m \frac{dC}{dT} + k^* C_w^* \gamma A$	A predictive model considering molecular diffusion, shear dispersion, and Brownian diffusion was developed to determine the wax deposition behavior in wellbores. It was demonstrated that at high temperature, molecular diffusion was dominant, while at low temperature, shear dispersion was dominant and the contribution of Brownian diffusion was smaller. The wax deposition model considering molecular diffusion and shear stripping was established, and the wax deposition tendency coefficient was also introduced, which proved that the deposition rate was the largest in the stable range of wax precipitation temperature and ambient temperature.
Hamouda [48]	MD, SD, ID	$\frac{dm_w}{dt} = -\frac{MW_w}{N_A} AD_m \frac{dC}{dT} \left( \frac{dT}{dr} \right)_{r=r_d}$	A semi-empirical model considering molecular diffusion and shear effects was proposed to predict the wax deposition process and distribution. It is proved that the turbulence effect had a significant impact on wax deposition. The concept of critical wax strength was proposed and it was suggested that it can be used as a reasonable scalar.
Hsu [49]	MD, SD	$\Omega = \left( \frac{k_m}{\mu} + f_s \right) \left( \frac{\rho_0 C_p}{4k_0} \right) \left( \frac{dC}{dT} \right)$	Based on the Svendsen model, the author believed that molecular diffusion, shear dispersion, and aging would affect the wax deposition process, but he noted that the effect of shear dispersion was small and could be ignored in the modeling process. The prediction results show that there were a lot of heavy components in the sedimentary layer, which was related to the prediction time and inlet distance.
Ramírez-Jaramillo [50]	MD, SD, ID	$M(t, z) = \sum_{i=1}^n M_i(t, L) = \sum_{i=1}^n 2\pi \int_0^t \int_0^z R_w J_{r_i} \Big _{r=R_w} dz dt$	A model applicable to predict the rate and amount of wax deposition under laminar flow conditions was developed based on the law of mass conservation. The results show that the driving force required for wax deposition was the main factor contributing to the temperature difference between deposited layers, which led to aging.
Singh [51–53]	MD, SS	$W = \frac{d\phi}{dt} = \frac{D_m}{(1-C)^2} \frac{dC}{dT} \frac{N_w}{R} (T_h - T_w)$	

Legend: MD—Molecular Diffusion, BD—Brownian Diffusion, SD—Shear Dispersion, SR—Shear Removal, SS—Shear Stripping, ID—Internal Diffusion (Aging).

In the Burger model,  $W_t$  is the rate of wax deposition,  $\text{kg}/(\text{m}^2 \cdot \text{s})$ ;  $\rho_r$  is the wax density,  $\text{kg}/\text{m}^3$ ;  $D_m$  is the diffusion coefficient,  $\text{m}^2/\text{s}$ ;  $C$  is the volume fraction concentration of wax in solution;  $A$  is the surface available for deposition,  $\text{m}^2$ ;  $r$  is the pipe radius,  $\text{m}$ ;  $k^*$  is the wax deposition rate constant;  $C_w^*$  is the volume fraction concentration of wax out of solution at the wall, and  $\gamma$  is the shear rate,  $\text{m}/\text{s}$ .

In the Hamouda model,  $m_w$  is the amount of wax deposition,  $\text{kg}$ ;  $t$  is the time,  $\text{h}$ ;  $T$  is the temperature,  $^\circ\text{C}$ ;  $A$  is the wax deposition area,  $\text{m}^2$ ;  $MW_w$  is the molecular weight of wax crystals;  $N_A$  is the Avogadro constant.



In the Hsu model,  $\Omega$  is the wax deposition tendency;  $f_s$  is friction to depict the shear effect;  $k_0$  is the oil thermal conductivity;  $k_m$  is the constants;  $\mu$  is the oil velocity, m/s;  $\rho_0$  is the wax density, kg/m<sup>3</sup>.

In the Ramírez-Jaramillo model,  $M(t, z)$  is the total amount of deposited mass at time  $t$  and distance from inlet  $z$ , kg;  $R_w$  is the pipe radius minus the width of the deposited wax layer, m;  $J_{ri}$  the radial mass flux of each component in the mixture.

In the Singh model,  $\phi$  is the mass fraction of sediment in the oil sample;  $\zeta$  is the thickness of the turbidite layer, m;  $N_u$  is Nusselt number;  $R$  is the circulating flow radius, m;  $T_h$  is the oil temperature at the center of the pipeline, °C. Huang [54], Eskin [55] and Quan et al. [56] also provided their new insights into the single-phase flow wax deposition model. However, it must be noted that available models tend to consider only some of the mechanisms affecting the wax deposition process, and the accuracy of model calculations cannot be guaranteed. Moreover, most models are established based on empirical and semi-empirical methods, and the actual application of the model prediction results is still a problem that needs to be addressed by the petroleum industry.

In the process of hydrocarbon exploitation, it is not only confined to single-phase flow, but often there are oil-gas, oil-water, and oil-gas-water coexistence conditions [57–59]. Since the applicable conditions and assumptions of the wax deposition model are various, it is necessary to establish different types of models to characterize wax deposition behavior in the wellbore. Compared with single-phase flow, the research on wax deposition in multi-phase flow is carried out later and is still in the initial stage [60]. At present, the study on wax deposition law of multi-phase system mainly focuses on oil-gas and oil-water two-phase flows. The effect of different flow patterns on wax deposition is mainly considered in oil-gas two-phase flow. The single-phase flow wax deposition mechanism was utilized for analyzing and modeling in oil-gas two-phase flow. The wax deposition models in the oil-gas two-phase flow were proposed by Elphingstone [61], Apte [62], Gong [63], and Duan [64], and Duan et al. [65], and the model is summarized in Table 2.

In the Elphingstone model,  $y$  is the thickness of solid wax deposited;  $t$  is time, s;  $\rho$  is the total fluid density, kg/m<sup>3</sup>;  $\hat{c}_p$  is average bulk fluid specific heat;  $D_{wo}$  is diffusion coefficient of wax in hydrocarbon;  $\rho^s$  is solid wax density, kg/m<sup>3</sup>;  $k$  is average bulk fluid thermal conductivity;  $T$  is time-averaged bulk temperature.

**Table 2.** Summary of oil-gas two-phase wax deposition models.

Researcher	Mechanism	Mathematical Model	Establishment and Characteristics of the Model
Elphingstone [61]	MD, SD	$\frac{\partial y}{\partial t} = \frac{\rho^2 \hat{c}_p D_{wo}}{2v_{z,avg} t \delta} \frac{\partial \omega(w)}{\partial T}$	Based on single-phase flow wax deposition, a model for predicting gas-liquid two-phase flow wax deposition was developed by considering the effects of diffusion and shear, which may be conservative in predicting wax deposition amount, although field data were not sufficient to draw reliable conclusions. The effects of wax deposition layer condensate content, shear stripping, and flow pattern on the wax deposition rate were considered, and a two-phase flow wax deposition model was established. The applicability and accuracy of the model for the high wax content system need further validation.
Apte [62]	SS	$\frac{d\delta}{dt} = -\frac{\Pi_1}{1+\Pi_2} D_w \frac{dC_w}{dT} \frac{dT}{dr}$	Based on Fick's law, the wax deposition model of gas-liquid two-phase flow was proposed considering the superficial velocity of gas and liquid phases, flow pattern, and Reynolds number. The experimental verification was carried out with high waxy crude oil and air as the medium, and the conclusion that the thickness of wax deposition layer under stratified flow and intermittent flow varied with the change of velocity of gas and liquid phases was obtained.
Gong [63]	MD	$\frac{d\delta}{dt} = k Re_{fp}^a \Pi^b \frac{1}{\mu_o} \frac{dC}{dT} \frac{dT}{dr}$	

Table 2. Cont.

Researcher	Mechanism	Mathematical Model	Establishment and Characteristics of the Model
Duan [64]	MD, SD	$\frac{d\delta_i}{dt} = \frac{1}{\rho_{\text{dep}} \bar{F}_w(t)} \left( -D_{\text{wo}} \frac{1}{l_\xi} \frac{dC}{d\xi} \Big _{\text{from oil to interface}} + D_{\text{eff}} \frac{1}{l_\xi} \frac{dC}{d\xi} \Big _{\text{from interface into deposit}} \right)$	<p>A mathematical model has been developed to predict the deposit thickness and the wax fraction of deposit in oil/gas stratified pipe flow using a unidirectional flow analysis of non-isothermal hydrodynamics and heat/mass transfer. Based on diffusivity and the solubility gradient at the oil–deposit interface at a different time, the reason that the deposit forming a crescent shape at the cross-section of pipe observed in different experiments was revealed.</p> <p>A wax deposition model of oil-gas two-phase stratified pipe flow based on molecular diffusion mechanism is developed. In the model, unidirectional flow analyses of momentum, heat, and mass transfer are presented. The cause of forming a crescent shape at the cross-section of the pipe was given, which was observed in different experiments.</p>
Duan [65]	MD, SD, IG	$\frac{dM}{dt} = 2\pi r_i \Delta L q_{m,\text{in}} = 2\pi r_i \Delta L \left( -D_{\text{wo}} \frac{\partial C}{\partial r} \Big _{r_i} \right)$	

Legend: MD—Molecular Diffusion, SD—Shear Dispersion, SS—Shear Stripping, ID—Internal Diffusion (Aging).

In the Apte model,  $D_w$  is the molecular diffusion coefficient,  $\text{m}^2/\text{s}$ ;  $\delta$  is the wax thickness,  $\text{m}$ ;  $C_w$  is the wax concentration,  $\text{wt}\%$ ;  $t$  is the time,  $\text{s}$ ;  $r$  is the radial distance,  $\text{m}$ ;  $\Pi_1$  is the wax deposition coefficient of the wall, which reflects the wax deposition caused by the oil content in the wax deposition layer and molecule diffusion such as turbulent mass transfer, and  $\Pi_2$  is the wall dewaxing coefficient, which reflects the wall dewaxing caused by shear dispersion. In the Gong model,  $\delta$  is the wax thickness,  $\text{m}$ ;  $k$ ,  $a$ ,  $b$  is the constant;  $\Pi$  is the characteristic parameter of flow pattern;  $\text{Re}_{\text{fp}}$  is the Reynolds number of the flow pattern;  $t$  is the time,  $\text{s}$ ;  $T$  is the temperature,  $^\circ\text{C}$ .

In the Duan model,  $\delta$  is deposit thickness,  $\text{m}$ ;  $\xi$  is coordinate in a bipolar system,  $\text{rad}$ ;  $\rho_{\text{dep}}$  is the density of deposited wax,  $\text{kg}/\text{m}^3$ ;  $\bar{F}_w$  is average wax fraction in the deposit,  $\text{wt}\%$ ;  $t$  is time,  $\text{s}$ ;  $D_{\text{wo}}$  is diffusivity wax in crude oil,  $\text{m}^2/\text{s}$ ;  $l_\xi$  is scale factors of the bipolar coordinate system;  $C$  is the cross-sectional area inside the pipe,  $\text{m}^2$ ;  $D_{\text{eff}}$  is effective diffusivity in the deposit,  $\text{m}^2/\text{s}$ .

In the Duan model,  $M$  is mass flux;  $r_i$  is the radial distance from the center to the oil-deposit interface;  $t$  is time,  $\text{s}$ ;  $\Delta L$  is the pipe length of wax deposit buildup,  $\text{m}$ ;  $D_{\text{wo}}$  is the wax diffusivity in oil,  $\text{m}^2/\text{s}$ ;  $C$  is the wax concentration of crude oil,  $\text{kg}/\text{m}^3$ ;  $r$  is the inner radius of the pipe,  $\text{m}$ . For the research of the oil-water two-phase flow, Couto et al. [66] proposed a wax deposition kinetic model in oil-water two-phase flow based on the single-phase model they developed. The essence of this model was to replace the physical properties of crude oil with those of oil-water mixture and substituted them into the existing single-phase wax deposition model, but the model did not consider the reverse-phase case. After investigating the Couto model, Bruno et al. [67] found that the accuracy of the Brinkman correlation equation used in the viscosity calculation was highest only when the emulsion water content was below 50%. Thus, Bruno et al. improved the model by calculating the emulsion viscosity using the Richardson correlation equation, and an empirical equation for sediment water content calculation was fitted based on the experimental results.

$$f_{w, \text{sed}} = 0.0283e^{2.4184} f_{w, \text{bulk}} \quad (2)$$

Here,  $f_{w, \text{sed}}$  is the water content of sediment,  $\%$ ;  $f_{w, \text{bulk}}$  is water content of oil-water mixture,  $\%$ . The Singh model and Hernandez model in single-phase flow were modified by Wang et al. [68]. The idea that the two-phase diffusion coefficient is a strong function of water content was proposed by considering molecular diffusion and shear dispersion,

and the oil-water two-phase wax deposition behavior under different flow conditions was predicted.

$$\frac{dh}{dt} = \frac{-D_{ow} \left| \frac{dC_d}{dT} \right|_L \times \left| \frac{dT}{dr_d} \right|_L \times [1 - \phi(M_{wow})] - J_{sow} \rho_d^{-1}}{M_{wow}} \quad (3)$$

where  $\frac{dh}{dt}$  is gelling deposition thickness change rate in two-phase oil–water flow, m/s;  $D_{ow}$  is diffusion coefficient of wax in the oil,  $m^2/s$ ;  $\left| \frac{dC_d}{dT} \right|_L$  is waxy crystals solubility coefficient in two-phase flow with a certain position,  $^{\circ}C^{-1}$ ;  $\left| \frac{dT}{dr_d} \right|_L$  is a radial temperature gradient in two-phase flow with a certain position,  $^{\circ}C/m$ ;  $M_{wow}$  is wax fraction in the gelling deposition of two-phase oil–water flow, %;  $J_{sow}$  is convective mass flux from bulk to interface in two-phase flow,  $kg/(m^2 \cdot s)$ ;  $\rho_d$  is the density of gelling deposition in two-phase flow,  $kg/m^3$ . The flow loop experiment was used to verify the simulation results of the proposed model. It was found that the error between the quantitative prediction results of the average wax deposition thickness rate and the experimental measurement results was less than 10%, which showed that the model can well adapt to the prediction of the actual wax deposition environment. Then, based on the mechanism of shear dispersion and shear stripping, Wang et al. [69] established an oil-water two-phase wax deposition model incorporating the variation of flow parameters from an energy perspective, and a quantitative method to distinguish between shear dispersion and shear stripping has been proposed at the same time.

$$\begin{aligned} \frac{\partial}{\partial t} M(t, L) &= 2\pi \int_0^L -D_w \rho_{wax} \cdot \left| \frac{dC_w}{dT} \right|_L \cdot \left| \frac{dT}{dr_w} \right|_L \cdot r_w \cdot \frac{1}{F_{wax}} dx \\ &- 2\pi \int_0^L \frac{-D_w \rho_{wax}}{1 + \frac{\alpha^2 F_{wax}^2}{1 - F_{wax}}} \cdot \left| \frac{dC_w}{dT} \right|_L \cdot \left| \frac{dT}{dr_w} \right|_L \cdot r_w \cdot \frac{1}{F_{wax}} dx \\ &+ 2\pi \int_0^L k \cdot \alpha \cdot S_w \cdot \left| \frac{dE_s}{dL} \right|_{r_w} \cdot \frac{\rho_{wax}}{r_w \cdot \mu \cdot \frac{\mu}{wax} \cdot 2.3} \cdot r_w \cdot \frac{1}{F_{wax}} dx \end{aligned} \quad (4)$$

Here,  $t$  is formation time of deposits, h;  $L$  is pipeline length, m;  $D_w$  is diffusion coefficient of wax in the oil,  $m^2/s$ ;  $\rho_{wax}$  is the density of wax,  $kg/m^3$ ;  $C_w$  is wax concentration, %;  $T$  is temperature, K;  $r_w$  is the distance from the pipe center to the surface of deposits, m;  $F_{wax}$  is wax content of/in wax deposits, %;  $\alpha$  is the aspect ratio of wax crystals;  $k$  is shearing coefficient;  $S_w$  is volume concentration of wax crystals on the deposits surface, equivalent to  $F_{wax}$ , %;  $E_s$  is shearing energy, J;  $\mu$  is the viscosity of waxy crude oil, Pa·s. Currently, wax deposition in multiphase systems is modeled by introducing some parameters into the single-phase flow model to characterize the flow and deposition distribution properties at different flow patterns [70,71]. However, the research of wax deposition model in oil-gas-water three-phase flow is still in the exploration stage. Based on the analysis of experimental results, Quan et al. [72] concluded that the deposition volume caused by gelation was positive correlation with the precipitated wax crystal concentration and gelation temperature, and negative correlation with the shear force. Therefore, the growth rate calculation model of the sediment layer thickness under the oil-gas-water three-phase system was established as follows:

$$\frac{d\delta}{dt} = k \cdot \tau^m \cdot \frac{1}{\mu} \frac{dC}{dT} \frac{dT^{n+1}}{dr} + k_g \cdot \tau^p \cdot (C - C_{int}) \exp\left(\frac{T_{pp}}{T_{int}}\right) \quad (5)$$

where  $\frac{d\delta}{dt}$  is the wax deposit thickness, m;  $\tau$  is the shear stress at the pipe wall, Pa;  $C$  and  $C_{int}$  are the wax molecular concentrations corresponding to temperature conditions at the oil flow center and the oil-sediment interface, respectively;  $T_{pp}$  is the gelation temperature of the oil,  $^{\circ}C$ ;  $T_{int}$  is the temperature at the oil-sediment interface,  $^{\circ}C$ ;  $\mu$  is the viscosity at the oil flow temperature, Pa·s;  $k, m, n, k_g, p$  are constant, of which  $k_g$  is the gelation coefficient, which is related to the oil properties and temperature conditions.



### 3. Experiment Characterization of Wax Precipitation and Deposition Behavior

The modeling characterization has been continuously improved and advanced, but it is still difficult to intuitively describe wax precipitation and deposition behavior. Experimental techniques have been developed along with the improvement of prediction models, and there are dozens of varied methods to characterize the precipitation and deposition behavior in hydrocarbon systems. The common experimental methods are shown in Table 3.

**Table 3.** Experimental methods of characterization wax precipitation and deposition.

Characterization Category	Name	Working Principle	Advantages	Disadvantages
Wax precipitation behavior	Microscopic observation method	Different media have different degrees of light absorption.	(i) Visual observation of wax precipitation temperature. (ii) Less sample consumption.	The effect of stress is not considered.
	Viscometry method	When the wax is precipitated, the viscosity of the oil sample will suddenly change.	(i) Low cost; (ii) Convenient operation.	Wax precipitation temperature can only be measured under normal pressure.
	Differential scanning calorimetry method	The precipitation of wax crystals is determined by the change in heat flow rate of the oil sample and the reference material.	(i) Convenient operation. (ii) Less time consumption. (iii) Quick response.	(i) The effect of pressure is not considered. (ii) Test result is small.
	Laser Scattering method	The laser will show different energy attenuation after passing through different media.	(i) High accuracy. (ii) Considering pressure.	(i) Light transmission of oil samples is required (ii) There are limitations for oil samples with high density and viscosity.
	Ultrasonic method	Ultrasonic waves propagate at different speeds in different media.	(i) High accuracy. (ii) Not limited by the color of the oil.	(i) Complex operation. (ii) Expensive cost. (iii) Poor stability.
Wax deposition behavior	Cold plate method	Using temperature difference of oil-plate.	(i) Convenient operation. (ii) Low cost and energy consumption.	(i) Poor stability. (ii) Does not reflect actual flow.
	Cold finger method	Using temperature difference of oil-wall.	(i) Convenient operation. (ii) Low cost and energy consumption.	(i) Poor stability. (ii) Does not reflect actual flow.
	Rotating disk method	Using temperature difference of oil-plate.	The shear rate was used as a sensitive factor.	Does not reflect actual flow.
	Flow Loop method	Controlling the oil-wall temperature difference by using the cooling medium in the air of the loop	(i) Realistic restoration of the shear flow field. (ii) Considering high pressure.	(i) Expensive cost. (ii) Difficult to clean the pipes after the experiment

#### 3.1. Experiment Characterization of Wax Precipitation Behavior

As the temperature decreases during the hydrocarbon lifting, the wax dissolved in the hydrocarbon in molecular form gradually precipitates as small grains [73–75]. The wax precipitation temperature and amount are important parameters to determine the occurrence of wax precipitation behavior.

##### 3.1.1. Microscopic Observation Method

In contrast to oil, wax crystals have a birefringence, and the image of wax crystals can be observed through the microscope after the orthogonally polarized light generated by the light source passes through the oil sample. Its principle is shown in Figure 3. The oil sample is cooled down, and the temperature corresponding to the appearance of wax crystals in the polarized light microscope is recognized as the wax precipitation temperature of the oil sample [76]. However, Shi and Li et al. [77,78] believed that this method mainly relied on visual observation of wax crystal precipitation and judgment of wax precipitation temperature, which was interfered with by man-made subjective factors. Additionally, the existence of impurities and defects in the glass slide would lead

to a little error in the observation results. With the development of microscopic image acquisition and processing technology, the results of the microscopic observation method are more accurate and reliable, and the analysis of wax crystal microscopic images focuses on quantitative characterization studies [79,80]. Japper-Jaafar and Bai et al. [81,82] used orthogonally polarized light microscopy to observe the first step point temperature of grain number growth in the images to determine the wax precipitation temperature.

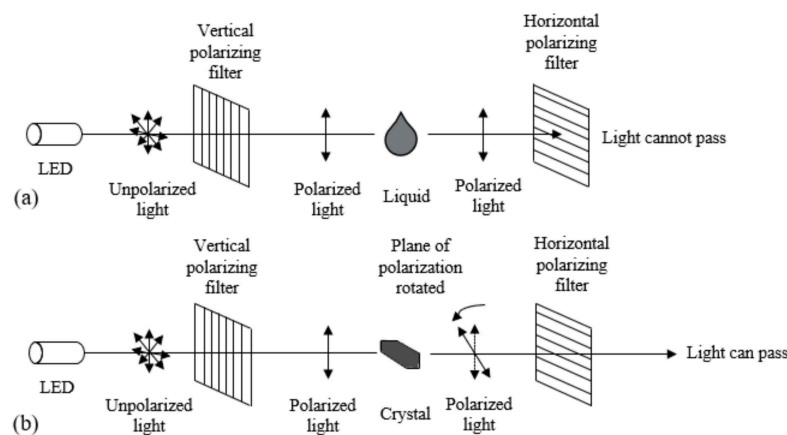


**Figure 3.** Schematic diagram of microscopic observation method principle. (a) homogeneous liquid and (b) crystalline material [83].

### 3.1.2. Viscometry Method

When measuring wax precipitation temperature by microscopic observation method, it is often affected by the transparency of the hydrocarbon system. Inspired by Escobedo et al. [84] using the viscometry method to measure asphaltene deposition temperature, the viscometry method was gradually used to determine wax precipitation temperature. The temperature corresponding to the sudden change in viscosity during the cooling process is considered as the wax precipitation temperature of the oil sample. In the study of Li, the wax precipitation temperature of five crude oils was measured by this method [78]. The wax content of the five crude oils ranged from 9.02% to 21.51%, and the rate of temperature drop during the experiment was 0.4 °C/min. The results showed that for crude oil with a slow initial wax precipitation rate and a low wax content, the variation of shear stress was slow under the effect of wax precipitation, so it was difficult to accurately determine the wax precipitation temperature of oil samples.

### 3.1.3. Differential Scanning Calorimetry Method

Differential scanning calorimetry (DSC) is the best thermal analysis technology with repeatability and quantification as it is based on the change in heat flow of the oil and the reference substance to determine whether wax crystals are precipitated. When no wax crystal appears in the oil sample to be measured, the heat flow curve varies slowly and gently [83]. When the wax crystals are precipitated, the latent heat of wax is released and the heat flow curve will suddenly increase to the maximum, at which time the corresponding temperature is the wax precipitation temperature [85]. The wax precipitation amount can also be measured by this method. Claudy et al. [86] employed the DCS method to measure the wax precipitation temperature of crude oil as early as 1988. Subsequently, a differential scanner was used to characterize the wax precipitation behavior of crude oil and surface condensate oil. The wax precipitation temperature was obtained, and it was also found that the wax precipitation amount increased with the decrease in temperature [87,88]. Additionally, the onset of wax crystallization and the rate of wax precipitation in waxy crude oils were also measured by the DSC technique in the study of Wang et al. [68], and also obtained the amount of wax precipitation at that temperature by plotting and analyzing DSC curves. However, Ronningsen et al. [89] argued that the differential scanner

could detect the variation of differential heat flow only when there was wax precipitation in the oil sample, so the measurement results are on the small side.

#### 3.1.4. Laser Scattering Method

When the hydrocarbon system is a single liquid phase, the transmittance is stable, when the system however converts from a single-liquid phase to a liquid-solid two-phase, that is, wax crystals begin to precipitate, the liquid phase system will not change the transmittance, but the precipitated wax crystals will scatter the light beam. The appearance and increase in wax crystals would lead to a dramatic decrease in the light beam transmittance. The measurement accuracy of this method is high, but the transparency of the oil sample will affect the performance of the measured results, so it is very suitable for the determination of wax precipitation temperature of condensate oil with high transparency [90]. The wax precipitation behavior in high-temperature and high-pressure condensate gas wells was characterized by using a solid-phase deposition tester with laser scanning in the research of Zhong et al. [91]. The results showed that when the system pressure was higher than dew point pressure, the pressure had little effect on wax precipitation temperature. When the pressure was close to dew point pressure, the wax precipitation temperature increased obviously with the decrease in pressure. When the system pressure was lower than the dew point pressure, the wax precipitation temperature decreased with the decrease in pressure, and it was also found that the dew point pressure of the system increased with the decrease in temperature.

#### 3.1.5. Ultrasonic Method

The variation of ultrasonic propagation medium density will determine its propagation speed and energy variation, which is manifested in the variations of the ultrasonic time difference, amplitude ratio, first wave frequency, and ultrasonic attenuation coefficient. When the wax crystals are precipitated from the oil sample, the single-phase system is transformed into a two-phase system, the scattering attenuation of the ultrasonic waves is enhanced, and the temperature when the first wave frequency suddenly increases is recognized as the wax precipitation temperature [78,92]. The ultrasonic method can determine the wax precipitation temperature under high pressure, and it is not affected by the color of the oil sample compared with the laser scattering method. However, the equipment of this method is expensive, and the operation is relatively complex.

To sum up, many comparative studies have been conducted on the common methods to characterize the wax precipitation temperature and amount. Hansen [85], Ronningsen [89], Pedersen [93], and Cazaux et al. [94] believed that the results measured by microscopic observation method were more accurate than those measured by viscometry method and DSC method when considering the characteristics of the glass slide and cooling rate, and the results of the research showed that the microscopic observation method yielded the highest wax precipitation temperature, DSC method was the middle, and viscometry method was the lowest. The microscopic observation method and the viscometry method have clear requirements on the wax content, which are not considered suitable for oil samples with slow initial wax precipitation rate and low wax content. For the wax precipitation temperature characterization of the pressurized hydrocarbon system, the DSC method, ultrasonic method, and laser scattering method are usually applied. The DSC method and laser scattering method are often selected to characterize wax precipitation behavior of condensate oil system, however, the laser scattering method has certain shortcomings when the ability to control the low temperature environment is required.

### 3.2. Experiment Characterization of Wax Deposition Behavior

The modeling is to predict the possibility and severity of wax deposition in the oilfield and thus establish effective deblocking strategy. However, many assumptions are made in establishing wax deposition models, which limits the application of the model.

Experimental methods not only can visually characterize wax deposition behavior but also can provide essential data for the development of wax deposition theory.

### 3.2.1. Cold Plate Method

The cold plate is an early experimental apparatus to study wax deposition, which consisted of a cold plate, a water bath, and a stirring device. Cole et al. [95] carried out experiments through a cold plate apparatus as early as 1960 to investigate wax deposition behavior in oil-water two-phase flow and demonstrated that the wax deposition amount was correlated with the cold plate surface characteristics. Subsequently, Hunt et al. [96] simulated wax deposition behavior in wellbores using a cold plate apparatus and found that sediment formation amount was correlated with surface roughness. Besides, Leontaritis et al. [97] investigated the wax deposition behavior under molecular diffusion and shear mechanisms by means of an invented dynamic cold plate, and the effect of shear rate on wax deposition rate was empirically correlated with shear stress. The structure of the cold plate is simple and the temperature difference of the oil and plate is relatively easy to control, but the stability of the equipment has been the main problem that hinders its wide application. Recently, Tinsley et al. [98] made up for the shortcomings of the traditional cold plate apparatus by setting the distance between the two cold plates to provide the required pressure and shear stress conditions, the schematic diagram of the device structure is shown in Figure 4. However, there are significant deficiencies in characterizing wax deposition behavior in the condensate hydrocarbon system due to the finite pressure provided by this apparatus.

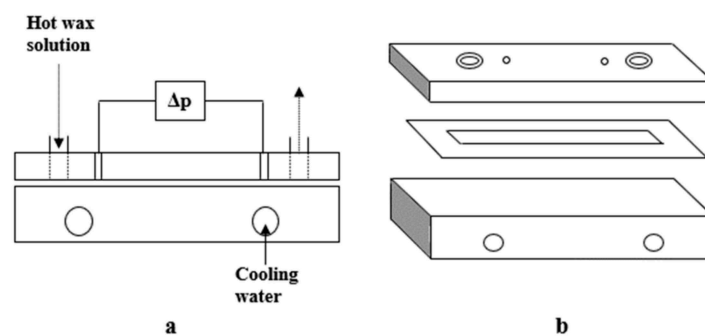


**Figure 4.** Schematic diagram of dynamic cold plate structure. (a) assembled deposition cell with direction of flow indicated by arrows, and (b) the upper plate, spacer and the lower plate that form the deposition channel [98].

### 3.2.2. Cold Finger Method

The cold finger is divided into two categories: static apparatus and dynamic apparatus. In the study of Bern and Weispfening et al. [99,100], the wax deposition in the hydrocarbon system was characterized using a static cold finger apparatus, which is shown in Figure 5a. Hamouda et al. [101] probed wax deposition in North Sea condensate oil by using a static cold finger apparatus and demonstrated that molecular diffusion was the major mechanism. It was concluded that as the system pressure increased, the lowest carbon value in the sediment decreased, while the lowest carbon number in the oil increased. The wax deposition behavior was also investigated utilizing static cold finger by Zhang [102], Kasumu [103], and Mahir et al. [104] However, the apparatus can only examine wax deposition when the hydrocarbon system was standing, which poorly reflects the real flow field. For this reason, Wang et al. [68] investigated the effect of water content on the carbon number distribution of sediment using a dynamic cold finger apparatus and found that the proportion of  $C_{17}$ - $C_{35}$  in the sediment decreased with increasing water content when the water content was greater than 30%. Subsequently, Wang et al. [69] determined the wax deposition rate under zero-shear and equivalent stirring conditions by a dynamic cold finger apparatus (Figure 5b). The oil-wall temperature difference was also controlled to ensure the molecular diffusion of the wax crystals, while the shear dispersion

coefficient was determined. Moreover, Zougari et al. [105] also improved the dynamic cold finger apparatus to perform single-phase, oil-gas, and oil-water two-phase wax deposition experiments under high-pressure and shear conditions (Figure 5c). It was found that the wax deposition rate of degassed crude oil is greater than that of gas-bearing crude oil. The improved dynamic cold finger apparatus also makes it a future addition to characterize the wax deposition behavior of waxy condensate oil in the wellbore.

### 3.2.3. Rotating Disk Method

The principle of the rotating disk method is similar to that of the cold plate method. The wax deposition behavior is characterized by measuring the amount of wax deposited on the metal disk within a specified time. The schematic diagram of apparatus is shown in Figure 6. Matlach et al. [106] employed the rotating disk method in measuring the wax deposition amount. The method allows control of oil temperature, rotating disk temperature, and rotation speed. This method is relatively easy to measure and control, but it is so inconsistent with the real shear flow field that it has rarely been used to characterize wax deposition behavior.

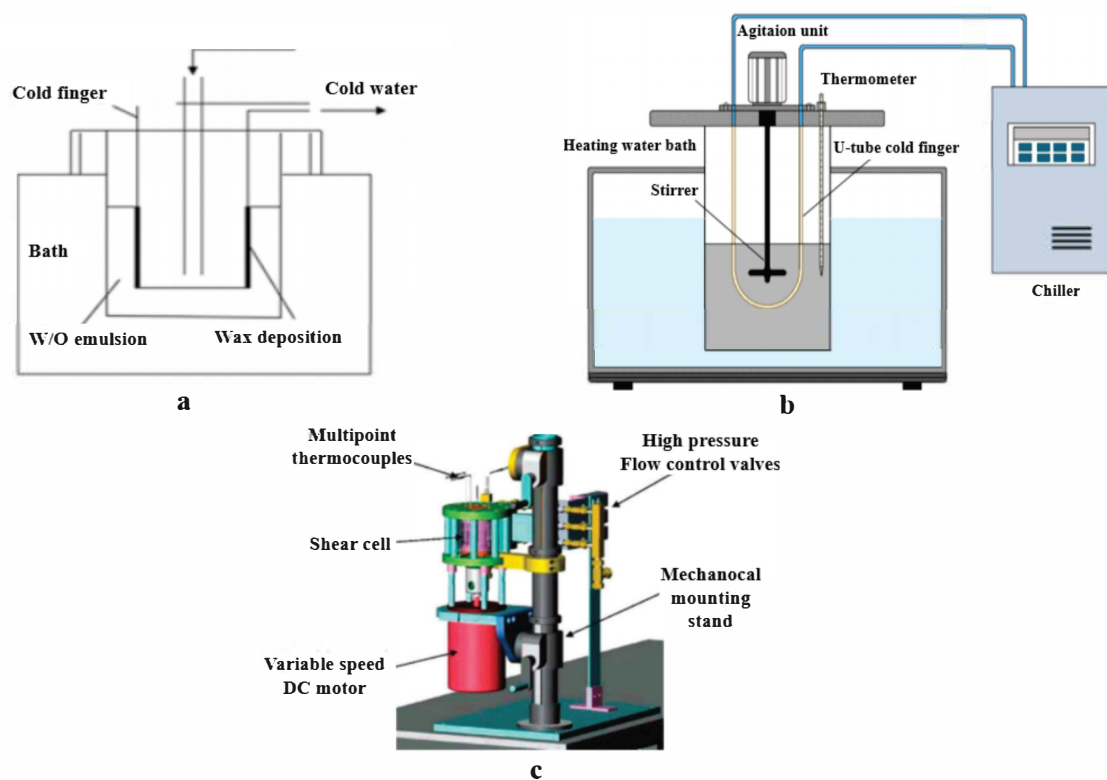


**Figure 5.** The schematic diagram cold finger apparatus. (a) static cold finger apparatus; (b) dynamic cold finger apparatus and (c) optimized dynamic cold finger apparatus [69,99,100,105].



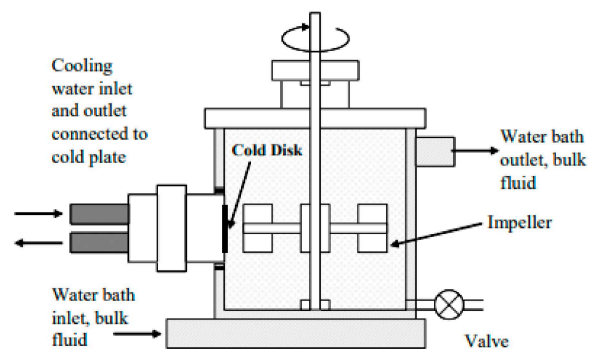


Figure 6. The schematic diagram of the stirred cell to measure wax deposition [107].

### 3.2.4. Flow Loop Method

Although flow loop experiment is the most expensive equipment to characterize wax deposition behavior, its characterization effect is the best. The flow field condition in the flow loop is similar to the actual hydrocarbon production and transportation process. Therefore, the study of wax deposition in the flow loop apparatus is more reliable than other deposition apparatuses. Its main components include: regulation system, pumping system, test section and deposit characterization devices [82]. The schematic of the flow loop apparatus is shown in Figure 7. Hsu et al. [49] established a high-pressure flow loop experimental apparatus to calculate the wax deposition by measuring the pressure difference between the test section and the reference section. Professor Bruno [67] of the University of Tulsa conducted a small-scale flow loop experiment of South Pelto crude oil and Garden Banks condensate oil, and concluded that the deposition thickness of both oil samples decreased with the increase in water content. Compared with the test results of South Pelto crude oil, the Garden Banks condensate oil with 85% water cut produced a very thin and hard sedimentary layer, which indicated that the sedimentary mechanism was different from the traditional diffusion theory. Hoffmann et al. [108] investigated wax deposition in single-phase flow at different temperatures and flow conditions with the condensate oil. The finding was that molecular diffusion was indeed the main mechanism controlling wax deposition, but an accurate quantitative description needs to take into account the effects of the deposited wax composition and shear stress. In addition, Ritirong et al. [109] performed wax deposition experiments on condensate oil under segment plug flow conditions using a pressurized flow loop apparatus and showed that the wax deposited thickness and quality were influenced by the variation of surface flow rate or phase flow rate.

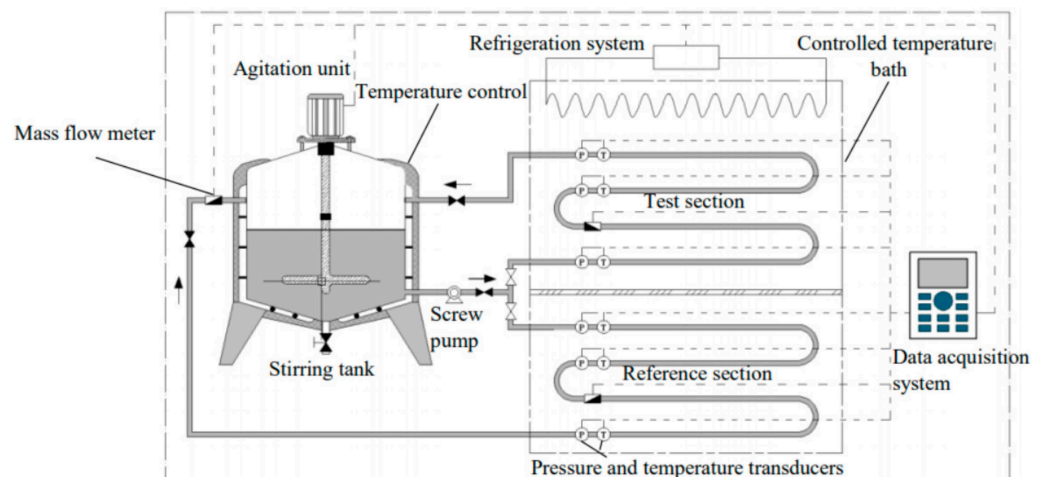
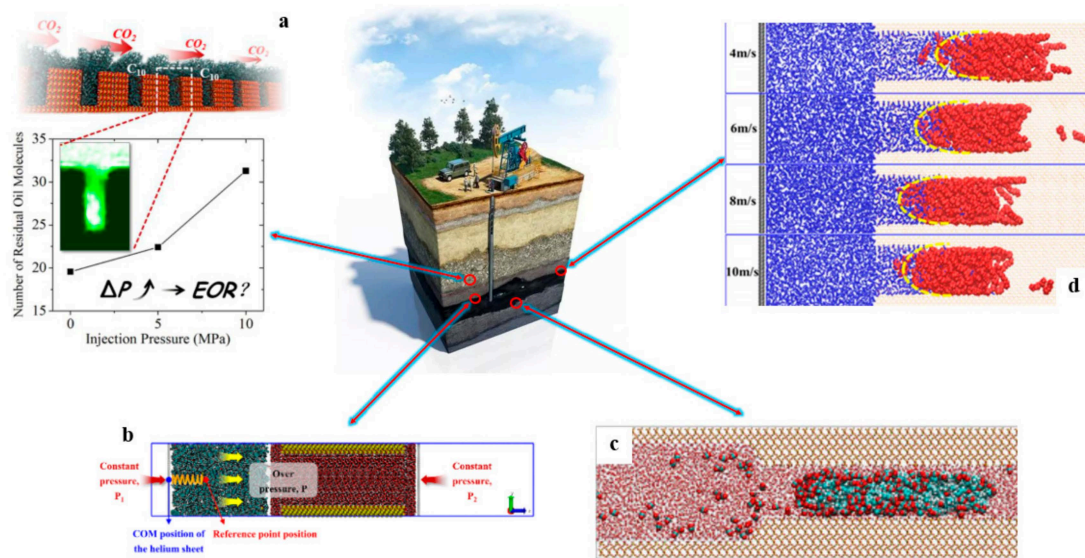


Figure 7. Schematic diagram of the flow loop apparatus [69].

From the above research, it is clear that the traditional cold plate and rotating disk methods are rarely used to characterize the wax deposition behavior due to certain defects. Currently, the cold finger method and flow loop method are still the most widely used characterization methods, which allow wax deposition experiments in pressurized systems. However, there are also some deficiencies in characterizing wax deposition behavior of condensate oil in the wellbore.

#### 4. Molecular Dynamics Characterization of Wax Precipitation and Deposition Behavior

In the hydrocarbon industry, Molecular dynamics (MD) simulation can provide significant contributions on upstream and downstream sectors. In terms of upstream hydrocarbon exploitation, computer-based studies are critical for the characterization of oil displacement processes, oil migration within the pore-throat, and oil droplet stripping mechanisms (Figure 8a–d). Fang et al. [110] theoretically discussed the molecular mechanism of viscoelastic polymer to enhance oil recovery. MD simulation was used to study the dynamic process of trapped oil droplet displacement from dead Angle in the nanopore. Zhang and his team [111–113] explained the mechanism and experimental phenomena of chemical oil flooding and supercritical CO<sub>2</sub> oil flooding at the molecular level, including the stripping mechanism of oil droplets, the effect of oil components, rock surface, and nanoparticles on the stripping of oil droplets, and the migration mechanism of oil in the pore-throat during CO<sub>2</sub> flooding and so on. These research topics contribute to the understanding of the underlying molecular processes, which are critical to improving hydrocarbon recovery mechanisms.



**Figure 8.** Schematic representation summarizing some upstream hydrocarbon industry systems investigated within the molecular modeling framework. (a) principle of carbon dioxide oil displacement; (b) initial model of the quartz nano-pore throat system and schematic diagram of the steered molecular dynamics simulation; (c) typical snapshots of process of with 200 CO<sub>2</sub> molecules at 5 ns; and (d) snapshots of the meniscus curvature at the same injection volume of CO<sub>2</sub> but different injection rates of 4, 6, 8 and 10 m/s [110–113].

In terms of downstream hydrocarbon gathering and treatment, MD simulation mainly focuses on emulsification and demulsification of produced liquid [114], film formation behavior at the oil-water interface [115], and hydrate treatment in low-temperature transportation. Gamba et al. [116] performed a pioneering investigation and proposed a “sandwich” structure to characterize the crude oil emulsion model, which was a lattice arrangement of a given oil and water molecule with a water layer in the middle and an oil layer on

both sides for a W/O emulsion, the reverse placement is assigned as the O/W emulsion. The role of sodium dodecylbenzene sulfonate (SDBS) in the separation of the oil-water interface was investigated by Li et al. by MD simulations [117], and it was found that SDBS molecules had an obvious inhibitory effect on the migration of water molecules near the interface, while water molecules far from the interface had a strong migration and diffusion ability. Li et al. [118] analyzed the effects of temperature, pressure, and initial concentration of methane in the liquid phase on the decomposition of methane hydrate in an aqueous environment by MD simulation method to further understand the hydrate dissociation mechanism at the microscopic level. At present, the relevant MD simulation researches mainly focus on the development and mechanism of action of wax inhibitors, while research on wax formation in the hydrocarbon system is still in its infancy. MD simulation as an emerging method for characterizing the wax precipitation and deposition behavior is gaining a lot of attention from petroleum workers.

#### 4.1. MD Simulation of Wax Precipitation Behavior

MD simulation techniques can effectively bridge the experimental gap and describe the microscopic behavior of wax phase transition and precipitation in terms of molecular motion, structure, and geometric changes at the nanoscale. MD simulation was applied to characterize the wax precipitation behavior in the study by Gan et al., Dodecane was used as the oil molecular model, and the mixture of  $C_{28}$  and  $C_{36}$  molecules was used as the wax molecular model; A force field model describing the molecular dynamics process of wax molecule and hydrocarbon mixture has also been established [119]. As shown in Figure 9, the microscopic process of wax molecules transforming from the irregularly dispersed state to larger gelled clusters in the oil system composed of a single hydrocarbon was demonstrated. While the number of wax crystals formed at different operating parameters was also analyzed by the density distribution in each direction. It was proved that the increase in temperature delayed the wax precipitation, and the increase in pressure and water content enhanced the solubility of wax molecules. Meanwhile, the formed emulsified water surface provided more bonding points for wax crystals, which strengthened the agglomeration and precipitation of wax crystals.

Subsequently, Chen et al. [120] characterized the wax precipitation behavior by comparing the self-diffusion coefficients and wax configurations between the two force fields, and also proved that the existence of wax molecules was one of the reasons for oil to inhibit molecular diffusion, where the wax molecular model consisted of a mixture of  $C_{26}$  and  $C_{38}$ . Wax molecules in the OPLS-AA force field crystallized when the temperature decreased, and some wax molecules aggregated when the temperature decreased to 313 K. The aggregated wax molecules tended to crystallize. However, no signs of crystallization were shown at any temperature in the APPLE&P force field and the wax molecules were uniformly distributed in the waxy hydrocarbon system. Simultaneously, the self-diffusion coefficient also validated this conclusion (Figure 10).

In Cao et al.'s latest research [121], the precipitation behavior of wax ( $C_{18}$ ,  $C_{18}+C_{28}$ ,  $C_{18}+C_{36}$ ) components in a single dodecane oil component model was characterized by MD simulation, and the wax precipitation temperature of the system was analyzed using radial distribution functions and self-diffusion coefficients based on the COMPASS force field. It was found that the wax molecules in the system gradually transformed from the dispersed state to the aggregated state as the temperature decreased, and the lower the temperature was, the easier the wax aggregated, and when the temperature was less than 313.15 K, the system underwent the phase transition process from liquid to solid (Figure 11). The results of the radial distribution functions and the self-diffusion coefficients also proved that the wax molecules underwent a phase transition at 313.15 K, i.e., the wax precipitation process.

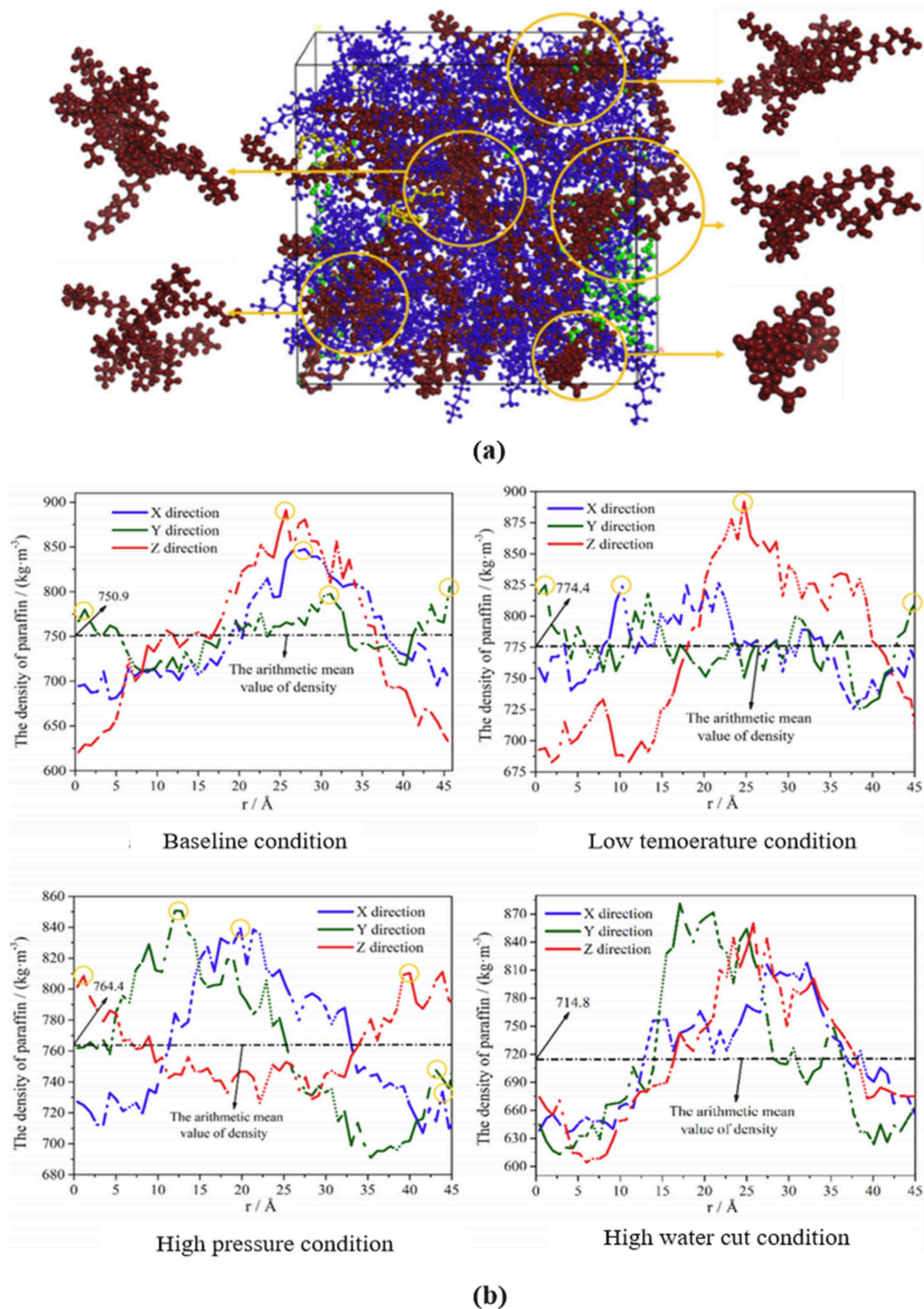


**Figure 9.** Schematic diagram of the final configuration of wax precipitation and density distribution of wax molecules in all directions. (a) final simulated configuration and (b) wax molecular density in X, Y and Z directions under different conditions [119].



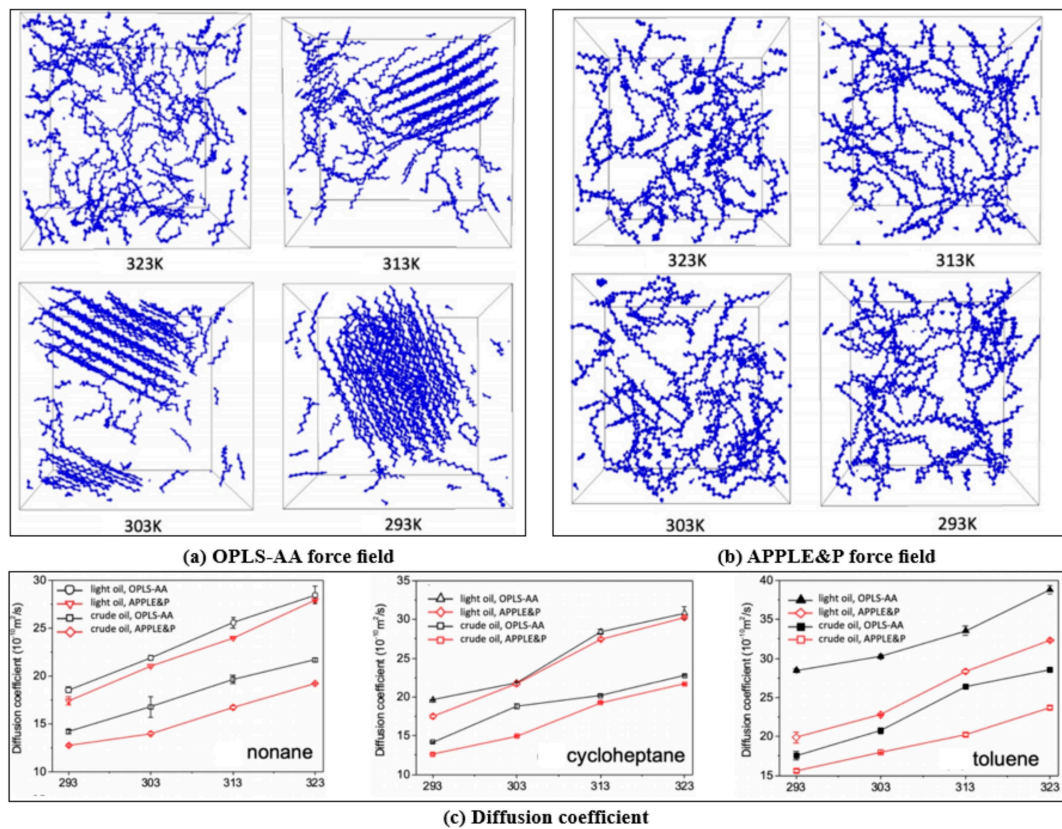


**Figure 10.** Configurations and self-diffusion coefficients of wax molecules from simulations with the OPLS-AA and APPLE&P force field. (a) simulation configuration of wax molecules at different temperatures based on OPLS-AA force field, (b) simulation configuration of wax molecules at different temperatures based on APPLE&P force field and (c) temperature dependence of diffusion coefficients of representative small molecules [120].

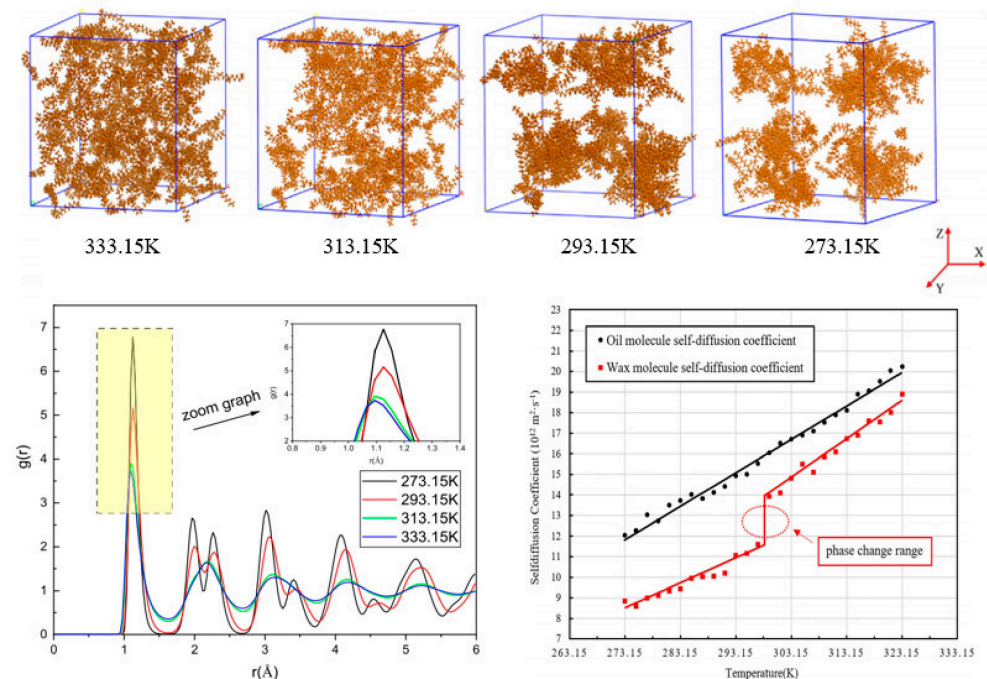


**Figure 11.** Schematic diagram of molecular dynamics characterization of precipitation behavior of wax molecules [121].



#### 4.2. MD Simulation of Wax Deposition Behavior

In order to characterize the microscopic deposition behavior of wax crystals, MD simulation techniques were incorporated. The processes related to the adsorption and deposition of wax molecules on the hematite surface were studied earlier by San-Miguel et al. [122]. It was found that the (0 0 1) surface of hematite was the surface that allowed the wax crystals to grow in the most favorable direction when wax molecules were randomly distributed on the hematite surface. The tendency for wax molecules to aggregate during the temperature drop was also observed. With the increase in the number of added wax molecules, different deposition layers were generated in the system, and the wax molecules had a clear trend of forming crystals. Gan et al. [123] established an oil-wall model to reveal the deposition and wall-sticking behavior of wax clusters in an oil system composed of a single  $C_{12}$  alkane based on the COMPASS force field, and found that the nucleation clusters first adhered to the wall to form a solidified oil layer. Then, wax molecules diffused to the deposition layer, and oil molecules in the solidified oil layer diffused backward toward the oil flow. With the increase in the adhesion and diffusion degree of clusters on the wall, the deposition layer gradually aged and formed a gel deposition layer with high density and hardness. At the same time, it is also found that the higher the surface free energy was, the better the hydrophilicity of the wall was, and the higher the adhesion degree of nucleation clusters on the wall was. In addition, the microscopic mechanism of the selective deposition process was also revealed by analyzing the microscopic information such as deposition location, binding conformation, and binding energy (Figure 12).

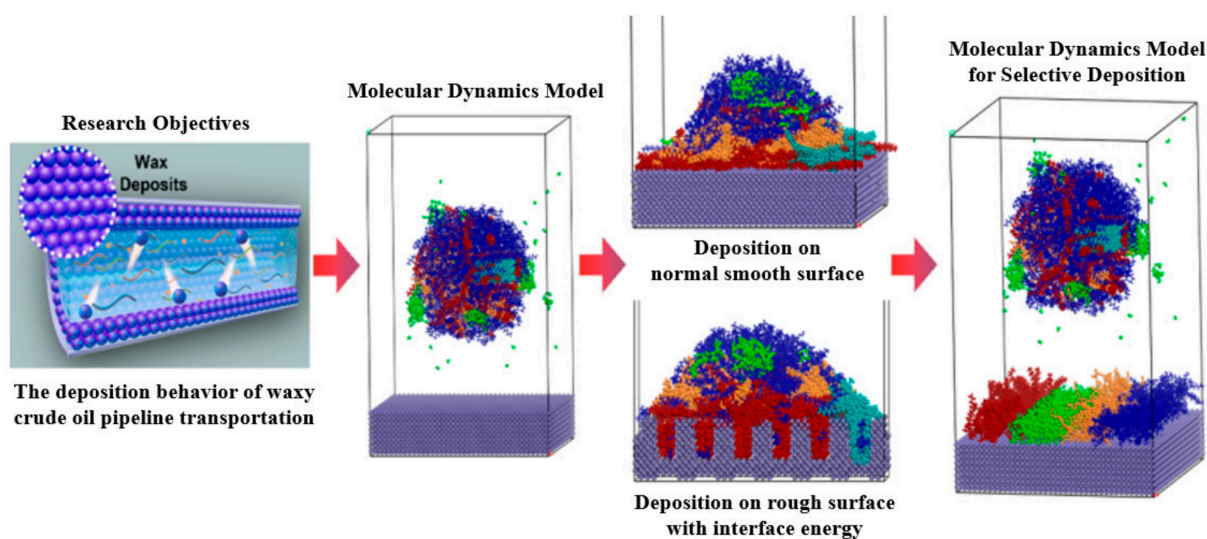


**Figure 12.** Schematic diagram of molecular dynamics characterization of wax molecules sticking on wall process [123].

In recent studies, Li et al. [124] took the pipe wall composed of copper molecules as the research object, and the waxy crude oil composed of oil molecules (dodecane), wax molecules (octadecane) and water molecules was modelled by OPSL-AA force field to simulate its deposition process on the pipe wall. It was found that at copper wall temperatures of 283 K, 293 K, and 303 K, the wax crystals formed a mesh structure on the copper wall, resulting in the gelation of waxy crude oil. The wax crystals tended to be horizontally aligned near the wall and vertically aligned away from the wall. The self-diffusion coefficient of wax molecules was smaller than the self-diffusion coefficient of oil molecules, which weakened the diffusion ability of oil molecules when wax molecules were present in the hydrocarbon system. The wax crystal formed a three-dimensional mesh structure in two regions, which wrapped the oil molecules and hindered the movement of oil molecules, thereby reducing the mobility of oil molecules and leading to the solidification of the hydrocarbon system (Figure 13).

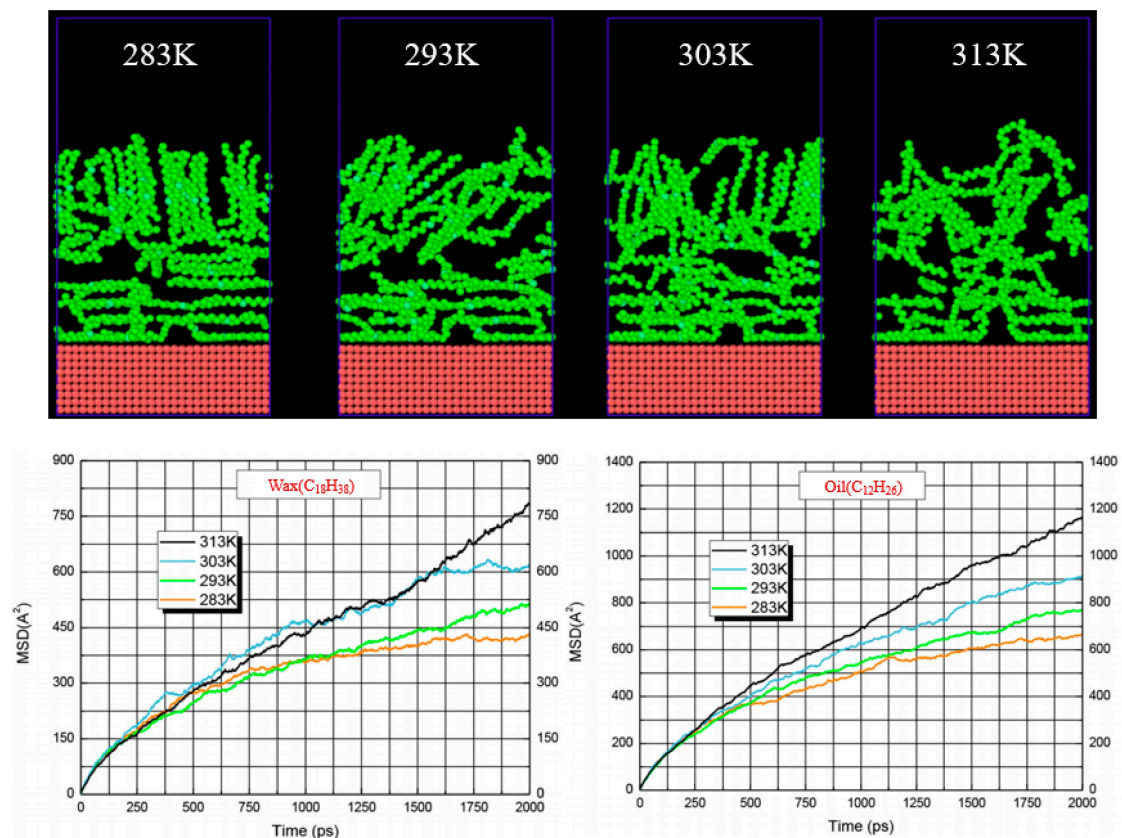


**Figure 13.** Schematic diagram of molecular dynamics characterization of wax deposition behavior [124].

## 5. Challenges and Prospects

It has been a common practice for a long time to reveal and characterize the wax precipitation and deposition behavior mainly by modeling and experiment means, the introduction of MD methods to deepen the description of phase transition and solid deposition has become a novel tendency, and the general idea of investigating wax precipitation and deposition behavior based on MD simulation has also been formed, the advantages and disadvantages of wax precipitation and deposition behavior characterization methods are shown in Figure 14. Nevertheless, in view of the characterization of wax precipitation and deposition behavior of condensate oil system in the wellbore, the following issues still need to be further addressed and investigated in terms of the improvement of predictive models, validation of macroscopic experiments, and expansion of MD simulation applications.

- (i) The above models can characterize the wax precipitation behavior of the condensate oil system with better accuracy. However, the models to predict the wax precipitation temperature and amount of the condensate oil may not give ideal results under certain extreme temperature and pressure conditions, such as deep reservoir forming environment at high temperature and high pressure.
- (ii) There are few experimental studies on the multi-phase flow wax deposition, and the experimental data obtained under different conditions are also scarce. It is also difficult to obtain the relevant data of wax deposition in the wellbore during the condensate oil production, which makes it difficult to provide sufficient data support for modeling and verification of wax deposition in condensate oil.
- (iii) Currently, the common experimental methods for characterizing wax deposition are still the cold finger method and the flow loop method. Although these characterization methods can be performed under the system with pressure, however, the maximum temperature and pressure values of the experimental apparatus are limited, and

the shear flow field cannot also be truly reflected. Hence, the experimental method for characterizing the wax deposition behavior of condensate in the wellbore has certain drawbacks.

- (iv) At present, most of the proven condensate oil is buried in deep and ultra-deep formations, and it is difficult to directly understand the wax precipitation and deposition behavior in the wellbore during development. Considering the safety and economy of working under high temperature and high pressure, it is also difficult to conduct large-scale experimental research in the laboratory. MD simulation technology is expected to become a new means to characterize the wax precipitation and deposition behavior of condensate oil in the wellbore, which can supplement and guide the predictive models and experimental studies, help to analyze the microscopic properties, and explain the macroscopic phenomena.
- (v) Considering the parallel calculation and calculation speed, it is inevitable to make appropriate simplifications to build the model, but the actual oil phase components are diverse, and the models containing a single hydrocarbon component are not conducive to the characterization of MD method to the microscopic behavior of wax precipitation and deposition of condensate oil in wellbore.
- (vi) During the condensate oil development, massive wax crystals are often precipitated and adhere to the wellbore wall due to variations in oil phase composition and external environment. Along with the existence of sand and scale, and the possibility of hydrate formation, the wellbore blockage is increasingly becoming serious. Therefore, how to effectively construct a method to characterize the coupled deposition behavior of wax and asphaltene, sand, scale, and hydrate at the microscale is the direction for further investigation and application of MD simulation in the future.

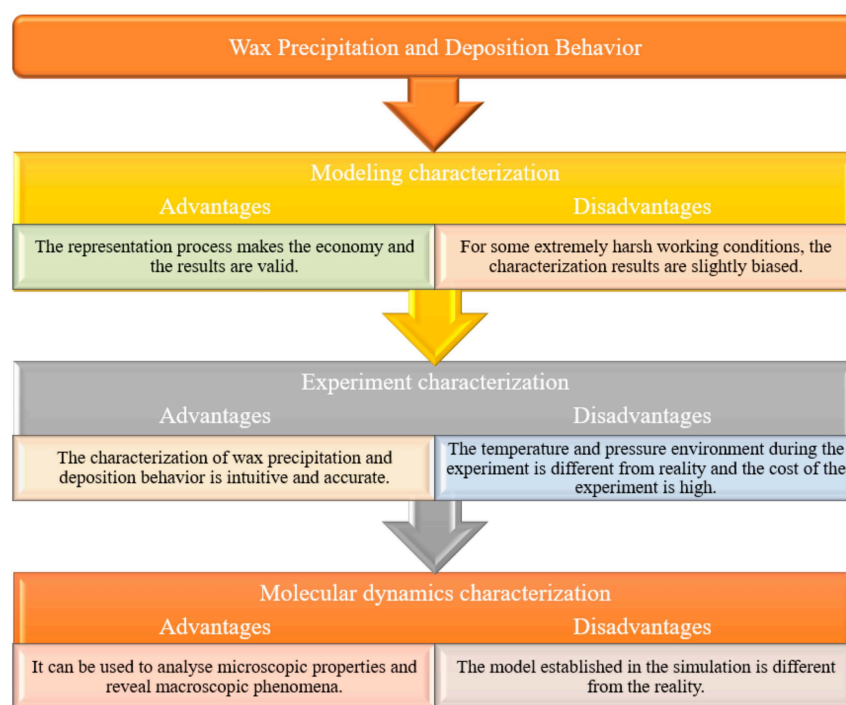


**Figure 14.** Analysis of wax precipitation and deposition behavior characterization means.

## 6. Conclusions

In the petroleum industry, wax precipitation and deposition are key challenges leading to flow limitation, productivity decline, and pipe plugging. This paper reviews characterization methods of wax precipitation and deposition behavior, analyses the applicability and limitations of wax precipitation prediction models, and argues that these models fall short in describing the wax precipitation behavior of condensate under specific extreme

external conditions. The research on wax deposition models of single-phase, two-phase and multi-phase flow has been progressively progressed, whereas the complex phase transition process of condensate oil in the wellbore makes the wax deposition behavior modeling characterization difficult to be accurately applied. The advantages, disadvantages and operational points of experimental characterization methods for wax precipitation and deposition behavior are summarized, and it is concluded that DSC and laser scattering methods are often used to characterize the wax precipitation behavior of condensate oil, and cold finger and flow loop methods are often used to characterize the wax deposition behavior. Furthermore, MD simulation is applied as an emerging method to characterize wax precipitation and deposition trouble. The application of this technology bridges the gap between modeling, experiment, and simulation, enriches the characterization methods of wax precipitation and deposition, and promote the development of unconventional hydrocarbon production and transportation technologies.

**Author Contributions:** Y.W. and X.L. performed the literature collection and induction. X.L. and Z.W. prepared the manuscript. Z.H. proofread and edited the manuscript. The whole work was supervised by Y.L. All authors have read and agreed to the published version of the manuscript.

**Funding:** This work presented in this paper was financially supported by the National Natural Science Foundation of China (Grant No. 52174060; 52074090) and Postdoctoral Scientific Foundation of Heilongjiang Province in China (Grant No. LBH-Q20012).

**Institutional Review Board Statement:** Not applicable.

**Informed Consent Statement:** Not applicable.

**Data Availability Statement:** The data presented in this review are available in article.

**Acknowledgments:** The authors gratefully acknowledge the support from the Heilongjiang Touyan Innovation Team Program, and the CNPC Innovation Foundation.

**Conflicts of Interest:** The authors declare no conflict of interest.

## References

1. McGlade, C.; Speirs, J.; Sorrell, S. Unconventional gas—A review of regional and global resource estimates. *Energy* **2013**, *55*, 571–584. [[CrossRef](#)]
2. Wang, H.; Ma, F.; Tong, X.; Liu, Z.; Zhang, X.; Wu, Z.; Li, D.; Wang, B.; Xie, Y.; Yang, L. Assessment of global unconventional oil and gas resources. *Pet. Explor. Dev.* **2016**, *43*, 925–940. [[CrossRef](#)]
3. Chen, C.; Wang, Y.; Beagle, J.R.; Liao, L.; Shi, S.; Deng, R. Reconstruction of the evolution of deep fluids in light oil reservoirs in the central tarim basin by using PVT simulation and basin modeling. *Mar. Pet. Geol.* **2019**, *107*, 116–126. [[CrossRef](#)]
4. Sheng, J.; Mody, F.; Griffith, P.J.; Barnes, W.N. Potential to increase condensate oil production by Huff-n-Puff gas injection in a shale condensate reservoir. *J. Nat. Gas Sci. Eng.* **2016**, *28*, 46–51. [[CrossRef](#)]
5. Wang, H.; Zhang, S.; Wang, N.; Li, W.; Qin, S.; Ma, W. Analysis of condensate oil by comprehensive two-dimensional gas chromatography-science direct. *Pet. Explor. Dev.* **2012**, *39*, 132–138. [[CrossRef](#)]
6. Wang, Z.; Liu, X.; Luo, H.; Peng, B.; Sun, X.; Liu, Y.; Rui, Z. Foaming properties and foam structure of produced liquid in alkali/surfactant/polymer flooding production. *J. Energy Resour. Technol.* **2021**, *143*, 103005. [[CrossRef](#)]
7. Chen, J.; Deng, C.; Wang, X.; Ni, Y.; Sun, Y.; Zhao, Z.; Wang, P.; Liao, J.; Zhang, D.; Liang, D. Source of condensate oil in the middle of southern margin, Junggar Basin, NW China. *Pet. Explor. Dev.* **2016**, *43*, 902–913. [[CrossRef](#)]
8. Weijermars, R.; Al-Shehri, D. Regulation of oil and gas reserves reporting in Saudi Arabia: Review and recommendations. *J. Pet. Sci. Eng.* **2022**, *210*, 109806. [[CrossRef](#)]
9. Wang, Y.; Ju, B.; Chen, W.; Zhang, K.; Ye, Y. Simulation-assisted gas tracer test study of Tarim Yaha gas-condensate reservoir in China. *J. Nat. Gas Sci. Eng.* **2017**, *48*, 77–84. [[CrossRef](#)]
10. Liu, Y.; Lu, H.; Liu, P.; Li, Y.; Wu, S.; Dai, P.; Yang, Q. Treatment of the complex liquid phase that contains produced water, condensate oil, and floccule from an offshore gas field: A pilot system for the South China Sea. *J. Nat. Gas Sci. Eng.* **2021**, *94*, 104125. [[CrossRef](#)]
11. Zhang, A.; Fan, Z.; Zhao, L. An investigation on phase behaviors and displacement mechanisms of gas injection in gas condensate reservoir. *Fuel* **2020**, *268*, 117373. [[CrossRef](#)]
12. Wang, J.; Zhou, F.; Zhang, L.; Huang, Y.; Yao, E.; Zhang, L.; Wang, F.; Fan, F. Experimental study of wax deposition pattern concerning deep condensate gas in Bozi Block of tarim oilfield and its application. *Thermochim. Acta* **2018**, *671*, 1–9. [[CrossRef](#)]
13. White, M.; Pierce, K.; Acharya, T. A review of wax-formation/mitigation technologies in the petroleum industry. *SPE Prod. Oper.* **2018**, *33*, 476–485. [[CrossRef](#)]



14. Ellison, B.T.; Gallagher, C.T.; Frostman, L.M.; Lorimer, S.E. The physical chemistry of wax, hydrates, and asphaltene. In Proceedings of the Offshore Technology Conference, Houston, TX, USA, 1–4 May 2000.
15. Oliveira, M.D.; Vieira, L.; Miranda, L.; Miranda, D.; Marques, L. On the influence of micro-and macro-cristalline paraffins on the physical and rheological properties of crude oil and organic solvents. *Chem. Chem. Technol.* **2016**, *10*, 451–458. [[CrossRef](#)]
16. Adebisi, F.M. Paraffin wax precipitation/deposition and mitigating measures in oil and gas industry: A review. *Pet. Sci. Technol.* **2020**, *38*, 962–971. [[CrossRef](#)]
17. Leontaritis, K.J. Wax flow assurance issues in gas condensate multiphase flowlines. In Proceedings of the Offshore Technology Conference, Houston, TX, USA, 30 April–3 May 2007.
18. Yang, F.; Chen, J.; Yao, B.; Li, C.; Sun, G. Effects of EVA additive dosage on rheological properties of asphaltenic waxy oils. *Acta Pet. Sin.* **2021**, *37*, 572–583.
19. El-Dalatony, M.M.; Jeon, B.H.; Salama, E.S.; Eraky, M.; Kim, W.B.; Wang, J.; Ahn, T. Occurrence and characterization of paraffin wax formed in developing wells and pipelines. *Energies* **2019**, *12*, 967. [[CrossRef](#)]
20. Nguyen, V.T.; Rogachev, M.K.; Aleksandrov, A. Nikolaevich. A new approach to improving efficiency of gas-lift wells in the conditions of the formation of organic wax deposits in the Dragon field. *J. Pet. Explor. Prod. Technol.* **2020**, *10*, 3663–3672. [[CrossRef](#)]
21. Labes-Carrier, C.; Ronningsen, H.P.; Kolnes, J.; Leporcher, E. Wax Deposition in North Sea Gas Condensate and Oil Systems: Comparison Between Operational Experience and Model Prediction. In Proceedings of the SPE Annual Technical Conference and Exhibition, San Antonio, TX, USA, 24–27 September 2002.
22. Rahimpour, M.R.; Davoudi, M.; Jokar, S.M.; Khoramdel, I.; Shariati, A.; Dehnavi, M.R. Wax formation assessment of condensate in south pars gas processing plant sea pipeline (a case study). *J. Nat. Gas Sci. Eng.* **2013**, *10*, 25–40. [[CrossRef](#)]
23. Gluyas, J.; Underhill, J.R. The staffa field, Block 3/8b, UK North Sea. *Geol. Soc. Lond. Mem.* **2003**, *20*, 327–333. [[CrossRef](#)]
24. Wang, Y.; Li, X.; Lu, J. Experimental study and numerical modeling of boron transport in reservoir and its influence on seawater-breakthrough calculation. *SPE Reserv. Eval. Eng.* **2021**, *24*, 292–309. [[CrossRef](#)]
25. Geest, C.; Melchuna, A.; Bizarre, L.; Bannwart, A.C.; Guersoni, V. Critical review on wax deposition in single-phase flow. *Fuel* **2021**, *293*, 120358. [[CrossRef](#)]
26. Sandyga, M.S.; Struchkov, I.A.; Rogachev, M.K. Formation damage induced by wax deposition: Laboratory investigations and modeling. *J. Pet. Explor. Prod. Technol.* **2020**, *10*, 2541–2558. [[CrossRef](#)]
27. Shoushtari, A.B.; Asadolahpour, S.R.; Madani, M. Thermodynamic investigation of asphaltene precipitation and deposition profile in wellbore: A case study. *J. Mol. Liq.* **2020**, *320*, 114468. [[CrossRef](#)]
28. Meighani, H.M.; Ghotbi, C.; Behbahani, T.J.; Sharifi, K. A new investigation of wax precipitation in Iranian crude oils: Experimental method based on FTIR spectroscopy and theoretical predictions using PC-SAFT model. *J. Mol. Liq.* **2018**, *249*, 970–979. [[CrossRef](#)]
29. Coutinho, J.A.P. Predictive UNIQUAC: A new model for the description of multiphase solid-liquid equilibria in complex hydrocarbon mixtures. *Ind. Eng. Chem. Res.* **1998**, *37*, 4870–4875. [[CrossRef](#)]
30. Coutinho, J.A.P.; Andersen, S.I.; Stenby, E.H. Evaluation of activity coefficient models in prediction of alkane solid-liquid equilibria. *Fluid Phase Equilibria* **1995**, *103*, 23–39. [[CrossRef](#)]
31. Yang, Y.; Lun, Z.; Wang, R.; Hu, W. Non-equilibrium phase behavior in gas condensate depletion experiments-sciencedirect. *Fluid Phase Equilibria* **2020**, *506*, 112410. [[CrossRef](#)]
32. Loskutov, V.Y.; Yadrevskaya, N.N.; Yudina, N.V.; Usheva, N.V. Study of viscosity-temperature properties of oil and gas-condensate mixtures in critical temperature ranges of phase transitions. *Procedia Chem.* **2014**, *10*, 343–348. [[CrossRef](#)]
33. Asbaghi, E.V.; Nazari, F.; Assareh, M.; Nezhad, M.M. Toward an efficient wax precipitation model: Application of multi-solid framework and PC-SAFT with focus on heavy end characterization for different crude types. *Fuel* **2022**, *310*, 122205. [[CrossRef](#)]
34. Góes, M.R.R.T.; Teixeira, R.G.D.; Tavares, F.W.; Secchi, A.R. Wax appearance and prevention in two-phase flow using the multi-solid and drift-flux model. *J. Pet. Sci. Eng.* **2019**, *177*, 374–383. [[CrossRef](#)]
35. Yang, J.; Wang, W.; Huang, H.; Shi, G.; Shi, B.; Cheng, B.; Gong, J. Prediction of solid-liquid equilibrium in paraffinic systems with new solid solution model. *Fluid Phase Equilibria* **2016**, *427*, 504–512. [[CrossRef](#)]
36. Won, K.W. Thermodynamics for solid solution-liquid-vapor equilibria: Wax phase formation from heavy hydrocarbon mixtures. *Fluid Phase Equilibria* **1986**, *30*, 265–279. [[CrossRef](#)]
37. Thomas, F.B.; Bennion, D.B.; Hunter, B.E. Experimental and theoretical studies of solids precipitation from reservoir fluid. *J. Can. Pet. Technol.* **1992**, *31*, 22–31. [[CrossRef](#)]
38. Lira-Galeana, C.; Firoozabadi, A.; Prausnitz, J.M. Thermodynamics of wax precipitation in petroleum mixtures. *AIChE J.* **1996**, *42*, 239–248. [[CrossRef](#)]
39. Pedersen, K.S. Prediction of cloud-point temperatures and amount of wax precipitation. *SPE Prod. Facil.* **1995**, *10*, 46–49. [[CrossRef](#)]
40. Pan, H.; Firoozabadi, A.; Fotland, P. Pressure and composition effect on wax precipitation: Experimental data and model results. *SPE Prod. Facil.* **1997**, *12*, 250–258. [[CrossRef](#)]
41. Nichita, D.V.; Goual, L.; Firoozabadi, A. Wax precipitation in gas condensate mixtures. *SPE Prod. Facil.* **1999**, *16*, 250–259. [[CrossRef](#)]
42. Nichita, D.V.; Pauly, J.; Montel, F.; Daridon, J.L. Pseudocomponent delumping for multiphase systems with waxy solid phase precipitation. *Energy Fuels* **2007**, *22*, 775–783. [[CrossRef](#)]



43. Daridon, J.L.; Pauly, J.; Coutinho, J.A.P.; Montel, F. Solid-liquid-vapor phase boundary of a North Sea waxy crude: Measurement and modeling. *Energy Fuels* **2001**, *15*, 730–735. [[CrossRef](#)]
44. Sansot, J.M.; Pauly, J.; Daridon, J.L.; Coutinho, J.A.P. Modeling high-pressure wax formation in petroleum fluids. *AIChE J.* **2005**, *51*, 2089–2097. [[CrossRef](#)]
45. Coutinho, J.A.P.; Edmonds, B.; Moorwood, T.; Szczepanski, R.; Zhang, X. Reliable wax predictions for flow assurance. *Energy Fuels* **2006**, *20*, 1081–1088. [[CrossRef](#)]
46. Zuo, J.; Zhang, D. Wax formation from synthetic oil systems and reservoir fluids. *Energy Fuels* **2008**, *22*, 2390–2395. [[CrossRef](#)]
47. Burger, E.D.; Perkins, T.K.; Striegler, J.H. Studies of wax deposition in the Trans Alaska pipeline. *J. Pet. Technol.* **1981**, *33*, 1075–1086. [[CrossRef](#)]
48. Hamouda, A.A.; Ravneoy, J.M. Prediction of wax deposition in pipelines and field experience on the influence of wax on drag-reducer performance. In Proceedings of the Offshore Technology Conference, Houston, TX, USA, 4–7 May 1992.
49. Hsu, J.J.C.; Santamaria, M.M.; Brubaker, J.P. Wax deposition of waxy live crudes under turbulent flow conditions. In Proceedings of the SPE Annual Technical Conference and Exhibition, New Orleans, LA, USA, 26–28 September 1994.
50. Ramirez-Jaramillo, E.; Lira-Galeana, C.; Brito, O.M. Numerical model for wax deposition in oil wells. *Pet. Sci. Technol.* **2001**, *19*, 587–608. [[CrossRef](#)]
51. Singh, P.; Fogler, H.S.; Nagarajan, N. Prediction of the wax content of the incipient wax-oil gel in a pipeline: An application of the controlled-stress rheometer. *J. Rheol.* **1999**, *43*, 1437–1459. [[CrossRef](#)]
52. Singh, P.; Youyen, A.; Fogler, H.S. Existence of a critical carbon number in the aging of a wax-oil gel. *AIChE J.* **2001**, *47*, 2111–2124. [[CrossRef](#)]
53. Singh, A.; Lee, H.S.; Singh, P.; Sarica, C. Flow assurance: Validation of wax deposition models using field data from a subsea pipeline. In Proceedings of the Offshore Technology Conference, Houston, TX, USA, 2–5 May 2011.
54. Huang, Z.; Lu, Y.; Hoffmann, R.; Amundsen, L.; Fogler, H.S. The effect of operating temperatures on wax deposition. *Energy Fuels* **2011**, *25*, 5180–5188. [[CrossRef](#)]
55. Eskin, D.; Ratulowski, J.; Akbarzadeh, K. Modelling wax deposition in oil transport pipelines. *Can. J. Chem. Eng.* **2014**, *92*, 973–988. [[CrossRef](#)]
56. Quan, Q.; Wu, H.; Gao, G. Wax deposition of single-phase waxy crude oil at different temperatures. *Oil Gas Storage Transport.* **2014**, *33*, 852–856.
57. Lin, X.; Wang, Z.; Feng, Q.; Zhang, L.; Xu, Y. The role of emulsified water in the wax deposition path of a waxy crude oil multiphase transportation pipeline. In Proceedings of the ASME Asia Pacific Pipeline Conference, Qingdao, China, 15–19 May 2019.
58. Wang, Z.; Wang, H.; Zhu, C.; Rui, Z.; Liu, Y. A novel method for characterizing the aggregation of wax crystals and an improvement in wax deposition modeling. *J. Energy Resour. Technol.* **2020**, *142*, 103003. [[CrossRef](#)]
59. Wang, Z.; Bai, Y.; Zhang, H.; Liu, Y. Investigation on gelation nucleation kinetics of waxy crude oil emulsions by their thermal behavior. *J. Pet. Sci. Eng.* **2019**, *181*, 106230. [[CrossRef](#)]
60. Mansourpoor, M.; Azin, R.; Osfouri, S.; Izadpanah, A.A.; Saboori, R. Experimental investigation of rheological behavior and wax deposition of waxy oil–disulfide oil systems. *Nat. Resour. Res.* **2019**, *28*, 1609. [[CrossRef](#)]
61. Elphinstone, G.M.; Greenhill, K.L.; Hsu, J.J.C. Modeling of multiphase wax deposition. *J. Energy Resour. Technol.* **1999**, *121*, 81. [[CrossRef](#)]
62. Apte, M.S.; Matzain, A.; Zhang, H.Q.; Volk, M.; Brill, J.P.; Creek, J.L. Investigation of paraffin deposition during multiphase flow in pipelines and wellbores-part 2: Modeling. *J. Energy Resour. Technol.* **2001**, *123*, 150–157. [[CrossRef](#)]
63. Gong, J.; Zhang, Y.; Liao, L.; Duan, J.; Wang, P.; Zhou, J. Wax deposition in the oil/gas two-phase flow for a horizontal pipe. *Energy Fuels* **2011**, *25*, 1624–1632. [[CrossRef](#)]
64. Duan, J.; Liu, H.; Guan, J.; Hua, W.; Jiao, G.; Gong, J. Wax deposition modeling of oil/gas stratified smooth pipe flow. *AIChE J.* **2016**, *62*, 2550–2562. [[CrossRef](#)]
65. Duan, J.; Li, J.; Liu, H.; Gu, K.; Guan, J.; Xu, S.; Gong, J. A model of wax deposition under oil-gas two-phase stratified flow in horizontal pipe. *Oil Gas Sci. Technol.* **2018**, *73*, 80. [[CrossRef](#)]
66. Couto, G.H.; Chen, H.; Dellecase, E.; Sarica, C.; Volk, M. An investigation of two-phase oil/water paraffin deposition. *SPE Prod. Oper.* **2008**, *23*, 49–55. [[CrossRef](#)]
67. Bruno, A.; Sarica, C.; Chen, H.; Volk, M. In paraffin deposition during the flow of water-in-oil and oil-in-water dispersions in pipes. In Proceedings of the SPE Annual Technical Conference and Exhibition, Denver, CO, USA, 21–24 September 2008.
68. Wang, Z.; Liu, Y.; Li, J.; Zhuge, X.; Zhang, L. Study on two-phase oil-water gelling deposition behavior in low temperature transportation. *Energy Fuels* **2016**, *30*, 4570–4582. [[CrossRef](#)]
69. Wang, Z.; Xu, Y.; Zhao, Y.; Li, Z.; Liu, Y.; Hong, J. Role of shearing dispersion and stripping in wax deposition in crude oil pipelines. *Energies* **2019**, *22*, 4325. [[CrossRef](#)]
70. Obaseki, M.; Paul, E. Dynamic modeling and prediction of wax deposition thickness in crude oil pipelines. *J. King Saud Univ.-Eng. Sci.* **2021**, *33*, 437–445. [[CrossRef](#)]
71. Kelechukwu, E.M.; Al-Salim, H.S.; Saadi, A. Prediction of wax deposition problems of hydrocarbon production system. *J. Pet. Sci. Eng.* **2013**, *108*, 128–136. [[CrossRef](#)]
72. Quan, Q.; Wang, W.; Duan, J.; Li, Q.; Ruan, C.; Gong, J. A study on wax deposition model in oil-gas stratified flows. In Proceedings of the 5th Asian Symposium on Computational Heat Transfer and Fluid Flow, Busan, Korea, 22–25 November 2015.

73. Xu, Q.; Wang, Y.; Jiang, Y.; Zhang, Q.; Bo, L.; Liu, Z. Application of coiled tubing paraffin removal technique in high pressure oil and gas well. *Petrochem. Ind. Appl.* **2017**, *36*, 83–85.
74. Zhu, C.; Liu, X.; Xu, Y.; Liu, W.; Wang, Z. Determination of boundary temperature and intelligent control scheme for heavy oil field gathering and transportation system. *J. Pipeline Sci. Eng.* **2022**, *1*, 407–418. [[CrossRef](#)]
75. Wang, H.; Xu, Y.; Shi, B.; Zhu, C.; Wang, Z. Optimization and intelligent control for operation parameters of multiphase mixture transportation pipeline in oilfield: A case study. *J. Pipeline Sci. Eng.* **2022**, *1*, 367–378. [[CrossRef](#)]
76. Xu, J.; Xing, S.; Qian, H.; Chen, S.; Wei, X.; Zhang, R.; Li, L.; Guo, X. Effect of polar/nonpolar groups in comb-type copolymers on cold flowability and paraffin crystallization of waxy oils. *Fuel* **2013**, *103*, 600–605. [[CrossRef](#)]
77. Shi, J. Application of thermal analysis in the study of wax precipitation process of crude oil. *Oil Gas Storage Transp.* **1993**, *12*, 6.
78. Li, H.; Zhang, J.; Chen, J. Comparison of different methods on determining wax appearance temperature of crude oils. *Oil Gas Storage Transp.* **2003**, *22*, 4.
79. Japper-Jaafar, A.; Bhaskoro, P.T.; Mior, Z.S. A new perspective on the measurements of wax appearance temperature: Comparison between DSC, thermomicroscopy and rheometry and the cooling rate effects. *J. Pet. Sci. Eng.* **2016**, *147*, 672–681. [[CrossRef](#)]
80. Yang, W.; Fu, C.; Du, Y.; Xu, K.; Balhoff, M.T.; Weston, J.; Lu, J. Dynamic contact angle reformulates pore-scale fluid-fluid displacement at ultralow interfacial tension. *SPE J.* **2020**, *26*, 1278–1289. [[CrossRef](#)]
81. Japper-Jaafar, A.; Bhaskoro, P.T.; Sean, L.L.; Sariman, M.Z.; Nugroho, H. Yield stress measurement of gelled waxy crude oil: Gap size requirement. *J. Non-Newton. Fluid Mech.* **2015**, *218*, 71–82. [[CrossRef](#)]
82. Bai, C.; Zhang, J. Effect of carbon number distribution of wax on the yield stress of waxy oil gels. *Ind. Eng. Chem. Res.* **2013**, *52*, 2732–2739. [[CrossRef](#)]
83. Huang, Z.; Zheng, S.; Fogler, H.S. *Wax Deposition: Experimental Characterizations, Theoretical Modeling, and Field Practices*; CRC Press: Hoboken, NJ, USA, 2016.
84. Escobedo, J.; Mansoori, G.A. Theory of viscosity as a criterion for detection of onset of asphaltene flocculation. In Proceedings of the Society of Petroleum Engineers, Richardson, TX, USA, 6 January 1996.
85. Hansen, A.B.; Larsen, E.; Pedersen, W.B.; Nielsen, A.B.; Rønningsen, H.P. Wax precipitation from North Sea crude oils. 3. Precipitation and dissolution of wax studied by differential scanning calorimetry. *Energy Fuels* **1991**, *5*, 914–923. [[CrossRef](#)]
86. Claudy, P.; Létouffé, J.M.; Chagué, B.; Orrit, J. Crude oils and their distillates: Characterization by differential scanning calorimetry. *Fuel* **1988**, *67*, 58–61. [[CrossRef](#)]
87. Cui, S.; Tang, Y.; Zhao, Y.; Yan, Z.; Wang, H. Study on prediction of wax deposition conditions in high temperature and high pressure condensate gas reservoir. *Pet. Reserv. Eval. Dev.* **2017**, *7*, 5.
88. Jiang, Z.; Hutchinson, J.M.; Imrie, C.T. Measurement of the wax appearance temperatures of crude oils by temperature modulated differential scanning calorimetry. *Fuel* **2001**, *80*, 367–371. [[CrossRef](#)]
89. Roenningsen, H.P.; Bjoerndal, B.; Hansen, A.B.; Pedersen, W.B. Wax precipitation from North Sea crude oils: 1. Crystallization and dissolution temperatures, and newtonian and non-newtonian flow properties. *Energy Fuels* **1991**, *5*, 895–908. [[CrossRef](#)]
90. Cai, H.; Huang, C. Experimental study on wax deposit of high-waxy condensate gas well. *Petrochem. Ind. Appl.* **2011**, *30*, 3.
91. Zhong, C.; Wang, J.; Liu, J.; Huang, Y.; Zhou, F.; Yang, X. Software simulation and experimental study on the law of wax deposition pattern in deep condensate gas. *J. Petrochem. Univ.* **2019**, *32*, 96–100.
92. Chen, H.; Yang, S.; Nie, X.; Wu, Y.; Ding, J.; Wang, Z. Ultrasonic detection and analysis of the wax participation in high waxy oilfield. *Chin. Sci. Bull.* **2015**, *60*, 8.
93. Pedersen, W.B.; Hansen, A.B.; Larsen, E.; Nielsen, A.B.; Roenningsen, H.P. Wax precipitation from North Sea crude oils. 2. Solid-phase content as function of temperature determined by pulsed NMR. *Energy Fuels* **1991**, *5*, 908–913. [[CrossRef](#)]
94. Cazaux, G.; Barre, L.; Brucy, F. Waxy crude cold start: Assessment through gel structural properties. In Proceedings of the SPE Annual Technical Conference and Exhibition, New Orleans, LA, USA, 27–30 September 1998.
95. Cole, R.J.; Jessen, F.W. Paraffin deposition. *Oil Gas J.* **1960**, *58*, 87–91.
96. Hunt, E.B. Laboratory study of paraffin deposition. *J. Pet. Technol.* **1962**, *4*, 1259–1269. [[CrossRef](#)]
97. Leontaritis, K.J.; Geroulis, E. Wax deposition correlation-application in multiphase wax deposition models. In Proceedings of the Offshore Technology Conference, Houston, TX, USA, 2–5 May 2011.
98. Tinsley, J.F.; Prud'homme, R.K. Deposition apparatus to study the effects of polymers and asphaltenes upon wax deposition. *J. Pet. Sci. Eng.* **2010**, *72*, 166–174. [[CrossRef](#)]
99. Bern, P.A.; Withers, V.R.; Cairns, R.J.R. Wax deposition in crude oil pipelines. In Proceedings of the Offshore Technology Conference and Exhibition, London, UK, 3–5 October 1980.
100. Weispfennig, K. Advancements in paraffin testing methodology. In Proceedings of the SPE International Symposium on Oilfield Chemistry, Houston, TX, USA, 13–16 February 2001.
101. Hamouda, A.A.; Viken, B.K. Wax deposition mechanism under high-pressure and in presence of light hydrocarbons. In Proceedings of the SPE International Symposium on Oilfield Chemistry, Houston, TX, USA, 2–5 March 1993.
102. Zhang, Y.; Gong, J.; Ren, Y.; Wang, P. Effect of emulsion characteristics on wax deposition from water-in-waxy crude oil emulsions under static cooling conditions. *Energy Fuels* **2010**, *24*, 1146–1155. [[CrossRef](#)]
103. Kasumu, A.S.; Mehrotra, A.K. Solids deposition from wax-solvent-water “Waxy” mixtures using a cold finger apparatus. *Energy Fuels* **2015**, *29*, 501–511. [[CrossRef](#)]

104. Mahir, L.H.A.; Vilas, B.F.C.; Ketjuntiwa, T.; Fogler, H.S.; Larson, R.G. Mechanism of wax deposition on cold surfaces: Gelation and deposit aging. *Energy Fuels* **2019**, *33*, 3776–3786. [[CrossRef](#)]
105. Zougari, M.; Jacobs, S.; Ratulowski, J.; Hammami, A.; Broze, G.; Flannery, M.; Stankiewicz, A.; Karan, K. Novel organic solids deposition and control device for live-oils: Design and applications. *Energy Fuels* **2006**, *20*, 1656–1663. [[CrossRef](#)]
106. Matlach, W.J.; Newberry, M.E. Paraffin deposition and rheological evaluation of high wax content altamont crude oils. In Proceedings of the SPE Rocky Mountain Regional Meeting, Salt Lake City, UT, USA, 22 May 1983.
107. Ahn, S.; Wang, K.S.; Shuler, P.J.; Creek, J.L.; Tang, Y. Paraffin crystal and deposition control by emulsification. In Proceedings of the SPE International Symposium on Oilfield Chemistry, Houston, TX, USA, 2–4 February 2005.
108. Hoffmann, R.; Amundsen, L. Single-phase wax deposition experiments. *Energy Fuels* **2010**, *24*, 1069–1080. [[CrossRef](#)]
109. Rittirong, A.; Panacharoensawad, E.; Sarica, C. An experimental study of paraffin deposition under two-phase gas-oil slug flow in horizontal pipes. In Proceedings of the Offshore Technology Conference, Houston, TX, USA, 4–7 May 2015.
110. Fang, T.; Zhang, Y.; Ma, R.; Yan, Y.; Dai, C.; Zhang, J. Oil extraction mechanism in CO<sub>2</sub> flooding from rough surface: Molecular dynamics simulation. *Appl. Surf. Sci.* **2019**, *494*, 80–86. [[CrossRef](#)]
111. Fang, T.; Zhang, Y.; Liu, J.; Ding, B.; Yan, Y.; Zhang, J. Molecular insight into the miscible mechanism of CO<sub>2</sub>/C10 in bulk phase and nanoslits. *Int. J. Heat Mass Transf.* **2019**, *141*, 643–650. [[CrossRef](#)]
112. Yan, Y.; Dong, Z.; Zhang, Y.; Wang, P.; Fang, T.; Zhang, J. CO<sub>2</sub> activating hydrocarbon transport across nanopore throat: Insights from molecular dynamics simulation. *Phys. Chem. Chem. Phys.* **2017**, *19*, 30439–30444. [[CrossRef](#)]
113. Liu, B.; Wang, C.; Zhang, J.; Xiao, S.; Zhang, Z.; Shen, Y.; Sun, B.; He, J. Displacement mechanism of oil in shale inorganic nanopores by supercritical carbon dioxide from molecular dynamics simulations. *Energy Fuels* **2017**, *31*, 738–746. [[CrossRef](#)]
114. Wang, Z.; Xu, Y.; Liu, Y.; Liu, X.; Rui, Z. Molecular dynamics-based simulation on chemical flooding produced emulsion formation and stabilization: A critical review. *Arab. J. Sci. Eng.* **2020**, *45*, 7161–7173. [[CrossRef](#)]
115. Xu, Y.; Wang, H.; Wang, Z.; Xu, Z.; Hong, J.; Sun, W. Microscopic mechanism of asphaltene and resin aggregation behavior to the stability of oil water interface. *J. Northeast. Pet. Univ.* **2021**, *45*, 90–101.
116. Gamba, Z.; Hautman, J.; Shelley, J.C.; Klein, M.L. Molecular dynamics investigation of a newtonian black film. *Langmuir* **1992**, *8*, 3155–3160. [[CrossRef](#)]
117. Li, Z.; Guo, X.; Wang, H.; Li, Q.; Yuan, S.; Xu, G.; Liu, C. Molecular dynamics simulation of anionic surfactant aggregation at the oil/water interface. *Acta Phys. Chim. Sin.* **2009**, *25*, 6–12.
118. Li, K.; Chen, B.; Song, Y.; Yang, M. Molecular dynamics simulation of the effects of different thermodynamic parameters on methane hydrate dissociation: An analysis of temperature, pressure and gas concentrations. *Fluid Phase Equilibria* **2020**, *516*, 112606. [[CrossRef](#)]
119. Gan, Y.; Cheng, Q.; Wang, Z.; Yang, J.; Sun, W.; Liu, Y. Molecular dynamics simulation of the microscopic mechanisms of the dissolution, diffusion and aggregation processes for waxy crystals in crude oil mixtures. *J. Pet. Sci. Eng.* **2019**, *179*, 56–69. [[CrossRef](#)]
120. Chen, X.; Hou, L.; Wei, X.; Bedrov, D. Transport properties of waxy crude oil: A molecular dynamics simulation study. *ACS Omega* **2020**, *5*, 18557–18564. [[CrossRef](#)]
121. Cao, J.; Liu, L.; Liu, C.; He, C. Phase transition mechanisms of paraffin in waxy crude oil in the absence and presence of pour point depressant. *J. Mol. Liq.* **2021**, *345*, 116989. [[CrossRef](#)]
122. San-Miguel, M.A.; Rodger, P.M. Simulation of deposition of wax to iron oxide surfaces. *Mol. Simul.* **2001**, *26*, 193–216. [[CrossRef](#)]
123. Gan, Y.; Cheng, Q.; Chu, S.; Wang, Z.; Luan, G.; Sun, W.; Liu, C.; Li, Q.; Liu, Y. Molecular dynamics simulation of waxy crude oil multiphase system depositing and sticking on pipeline inner walls and the micro influence mechanism of surface physical–chemical characteristics. *Energy Fuels* **2021**, *35*, 4012–4028. [[CrossRef](#)]
124. Li, Q.; Deng, X.; Liu, Y.; Cheng, Q.; Liu, C. Gelation of waxy crude oil system with Ethylene-Vinyl Acetate on solid surface: A molecular dynamics study. *J. Mol. Liq.* **2021**, *331*, 115816. [[CrossRef](#)]